Atmos. Meas. Tech. Discuss., 7, 2017–2069, 2014
www.atmos-meas-tech-discuss.net/7/2017/2014/
doi:10.5194/amtd-7-2017-2014

Atmospheric Measurement Techniques Discussions
Open Access

Online technique for isotope and mixing ratios of CH_4, N_2O, Xe and mixing ratios of organic trace gases on a single ice core sample

J. Schmitt, B. Seth, M. Bock, and H. Fischer

Climate and Environmental Physics, Physics Institute & Oeschger Centre for Climate Change Research, University of Bern, Switzerland

Received: 13 December 2013 – Accepted: 14 February 2014 – Published: 3 March 2014

Correspondence to: J. Schmitt (schmitt@climate.unibe.ch)

Published by Copernicus Publications on behalf of the European Geosciences Union.

Abstract

Polar ice cores enclosing trace gas species offer a unique archive to study changes in the past atmosphere and in terrestrial/marine source regions. Here we present a new online technique for ice core and air samples to measure a suite of isotope ratios and mixing ratios of trace gas species on a single small sample. Isotope ratios are determined on methane, nitrous oxide and xenon with reproducibilities for ice core samples of 0.15 ‰ for δ^{13}C-CH_4, 0.22 ‰ for δ^{15}N-N_2O, 0.34 ‰ for δ^{18}O-N_2O, and 0.05 ‰ for δ^{136}Xe. Mixing ratios are determined on methane, nitrous oxide, xenon, ethane, propane, methyl chloride and dichloro-difluoromethane with reproducibilities of 7 ppb for CH_4, 3 ppb for N_2O, 50 ppt for ^{136}Xe, 70 ppt for C_2H_6, 70 ppt for C_3H_8, 20 ppt for CH_3Cl, and 2 ppt for CCl_2F_2. The system consists of a vacuum extraction device, a preconcentration unit and a gas chromatograph coupled to an isotope ratio mass spectrometer. CH_4 is combusted to CO_2 prior to detection while we bypassed the oven for all other species. The highly automated system uses only ~ 160 g ice, equivalent to ~ 16 mL air, which is less than previous methods. This large suite of parameters on a single ice sample is new and helpful to study phase relationships of parameters which are usually not measured together. A multi-parameter dataset is also key to understand in situ production processes of organic species in the ice, a critical issue observable in many organic trace gases. Novel is the determination of xenon isotope ratios using doubly charged Xe ions. The attained precision for δ^{136}Xe is suitable to correct the isotopic ratios and mixing ratios for gravitational firn effects, with the benefit that this information is derived from the same sample. Lastly, anomalies in the Xe mixing ratio, δXe/air, can be used to detect melt layers.

1 Introduction

The analysis of atmospheric trace gases and their stable isotopic ratios on air archived in ice cores is fundamental to reconstruct and understand the composition of the

AMTD
7, 2017–2069, 2014

atmosphere of the past. Of special interest are studies dealing with the greenhouse gases CO_2, N_2O, and CH_4 due to their radiative forcing. While the long-term temporal changes of their mixing ratios during the past 800 kyr (1 kyr = 1000 years) are broadly known, and in more detail for the last 140 kyr (Loulergue et al., 2008; Lüthi et al., 2008; Schilt et al., 2010), untangling the processes driving these changes remains a challenge. Here, the stable isotopic signatures help to track changes in the atmospheric budget, i.e. distinguish among sources and sink processes (Sowers et al., 2003; Ferretti et al., 2005; Bock et al., 2010b; Schmitt et al., 2012). For example, N_2O emitted from the ocean is enriched in both $\delta^{15}N$ and $\delta^{18}O$ compared to emissions from terrestrial ecosystems (Rahn and Wahlen, 2000); likewise CH_4 emitted from biomass burning carries a heavy $\delta^{13}C$ signature compared to microbial CH_4 (Whiticar and Schaefer, 2007). Again, for CO_2, organic carbon derived from terrestrial and marine ecosystems is strongly depleted compared to the carbon dissolved in the ocean. On the other hand, the wide natural variability of a particular source signature often leads to overlaps among sources, and source signatures may change through time (Möller et al., 2013). Besides these traditional trace gases at ppm (CO_2) or ppb levels (CH_4 and N_2O), atmospheric trace gases in the ppt level, like CO, ethane, propane or methyl chloride, are currently being explored in firn (Aydin et al., 2011; Worton et al., 2012) and ice core studies (Saltzman et al., 2009; Wang et al., 2010; Verhulst et al., 2013). Although these ppt-level gases do not significantly influence climate via the greenhouse effect, they act indirectly, e.g. modifying the lifetime of CH_4 via atmospheric chemistry. Trace gases like ethane, propane, and methyl chloride are predominantly emitted by plants and biomass burning (Pozzer et al., 2010; Xiao et al., 2010). Although not entirely specific for a certain emission type, these trace gases help to constrain possible scenarios in conjunction with other gas species and proxies. For example, methyl chloride shares similarities with CH_4, as the sources of methyl chloride are also located mostly in tropical regions and the life times of both gases are determined by tropospheric OH as their dominant sink. A challenge for most ppt-level gases and so far limiting their full usage in ice core research is the fact that production of these species in the ice itself (in situ

AMTD
7, 2017–2069, 2014

production) complicates the atmospheric reconstruction (Aydin et al., 2007; Faïn et al., 2013). Like in the case of CO_2, where records from Greenland ice cores have been shown to be obscured by in situ production (Tschumi and Stauffer, 2000), conditions favouring in situ production for N_2O, CH_4, and trace gases like ethane, propane, and methyl chloride have to be identified.

To analyse isotopes of CH_4 and N_2O on ice core samples, several methods using different extraction techniques have been developed (Sowers et al., 2005; Schaefer and Whiticar, 2007; Behrens et al., 2008; Melton et al., 2011; Sapart et al., 2011; Sperlich et al., 2013). In contrast, only a few techniques for ice core samples have been established to analyse trace gas species at the ppt level, such as for ethane, propane, and methyl chloride (Aydin et al., 2002; Saito et al., 2006; Aydin et al., 2007). Here, we present a new, multi-parameter method to simultaneously measure the mixing ratios and stable isotopic ratios of CH_4 and N_2O, the mixing ratios of ethane, propane, and methyl chloride and, additionally, the mixing ratio and isotopic ratio of Xe. This large suite of parameters requires a sample size of only ~ 160 g ice, which is considerably less than previous methods: a great asset in ice core research, where sample availability is highly limited. Besides sample consumption, deriving all parameters on the same sample is crucial to identify processes within the ice, like in situ production of trace gas species. For CH_4, these processes have been shown to occur in core sections affected by surface melting (NEEM community members, 2013) or are associated to sharp spikes associated with aerosol events from biomass burning (Rhodes et al., 2013). In both cases sample size is a critical parameter, and the combined knowledge from many gas species is crucial to identify the underlying processes affecting the archived atmospheric composition of the particular ice core sections.

2 Experimental set-up

Our set-up allows for quantitative extraction and measurement of a large suite of gas species (isotope ratios and/or mixing ratios) in ice and air samples. The set-up shown in

AMTD
7, 2017–2069, 2014

Fig. 1 comprises a custom-built online preconcentration system, combining a vacuum melt-extraction and a trapping line (Sect. 2.1) including a gas chromatographic separation line (Sect. 2.2). Via an open split this unit is coupled with the detection system, an isotope ratio mass spectrometer (IRMS) described in Sect. 2.3.

2.1 Vacuum extraction and trapping line

The extraction and trapping of the enclosed air of ice samples is carried out under vacuum conditions. The target gases are separated from H_2O, CO_2, and bulk air components (N_2, O_2, Ar) using individual trapping steps.

2.1.1 Sample vessel and melting device

Our sample vessel (~ 350 mL, DN63CF, MCD Vacuum Ltd., UK; Fig. 2) consists of a rounded-bottom glass part and a stainless steel (SST) flange and holds up to 260 g ice. A capillary (SST, o.d. 1/16″, i.d. 0.030″) reaching the bottom of the vessel provides the inlet for the reference gas and purge-He (Fig. 2). The vessel can be placed into a cooling-melting device – a plexiglas cylinder that can be automatically cooled to freezing temperatures using a liquid nitrogen (LN_2) pump (Schmitt, 2006; Schmitt et al., 2011) or heated using infrared radiation to melt the ice. An insulating styrofoam lid and fan guarantee a homogeneous temperature distribution throughout the cylinder.

The sample vessel can be bypassed using a 1/16″ capillary (SST, i.d. 0.030″). The bypass is used for reference gas measurements and air samples and allows tests in which the sample vessel is excluded from the flow path. These gases pass an SGE valve (SGE Analytical Sciences Pty. Ltd., Australia; Fig. 1), which allows us to simulate different sample sizes by changing the time the valve is opened.

2.1.2 Ice melting and trapping processes

The ice is melted using infrared radiation (Fig. 2). As a precaution against possible photochemical reactions of ultraviolet (UV) light with organic material (Vigano et al., 2009),

AMTD
7, 2017–2069, 2014

the short wave part of the emitted light, $\sim$< 600 nm, is absorbed by a UV blocker foil (Schmitt et al., 2011). During the melting process, which lasts $\sim$ 24 min, valves V1, V3, and V5 (diaphragm sealed valves, Swagelok) are open (Fig. 1). The released air is dried by freezing out water vapour in the *water trap* (SST tubing, o.d., 1/4″, 8 cm long, i.d. 0.209″) held at −80 °C. Between the sample vessel and the *water trap* we installed a restriction (SST, length 3 cm, i.d. 0.030″) to adjust the conductivity. We set it to optimise pumping efficiency while limiting excessive water from entering the *water trap*. Low pressure is the main advantage of continuous vacuum extraction compared to melting under He overpressure and is necessary to extract gases with high Henry coefficients at high extraction efficiency (Kawamura et al., 2003; Sperlich et al., 2013). During the melting of the ice sample the total pressure in the vessel (sum of partial pressures of H_2O and air) ranges between 12 mbar at the start and 7 mbar at the end. As the water temperature is close to 0 °C, resulting in a pH_2O of around 6 mbar, the partial pressure of air in the vessel is in the range of only 1 to 6 mbar. For comparison, melt extraction techniques, which melt the ice under He overpressure with closed valves (e.g. Behrens et al., 2008 and Bock et al., 2010a), produce air partial pressures $\sim$ 20 times larger than our values. Equally important to minimise the dissolution of gases into the water during melting is the total pressure as it determines the internal pressure of the rising bubbles in the meltwater.

Sample CO_2 is removed from the air stream by an Ascarite trap (10–35 mesh, Sigma-Aldrich, in 6 cm 1/4″ SST tubing, i.d. 0.085″). All other gases, besides He and Ne, are trapped on our *AirTrap* at −180 °C (SST, 12 cm, o.d. 1/8″, i.d. 0.085″ filled with activated carbon). During the melting process valves V2, V4, and VL1 remain closed. At the end of the melting process the sample vessel is cooled to +3 °C to keep the water vapour pressure low. He is then sent to flow through via the SGE valve into the bottom of the vessel ("purge-He", Fig. 1) and bubbled through the meltwater for approximately 14 min at a flow rate of 4 mL min^{-1} at STP (standard temperature and pressure); VL1 and VL3 are open. We thereby we expel the remaining air from the vessel headspace and the tubing towards the *AirTrap* to achieve quantitative collection.

AMTD
7, 2017–2069, 2014

Simultaneously, the *AirTrap* is heated to a temperature of −78 °C to keep the gases of interest adsorbed on the activated carbon while the bulk air components (N_2, O_2, and Ar) are flushed out with the He flow. The extraction and trapping step ends when the *AirTrap* is switched into the GC line using valve 1 (Fig. 1; 6-port Vici Valco, Vici AG International, Switzerland).

2.1.3 Re-collection of the bulk air

Determining the amount of air corresponding to the trace gas species is necessary in order to calculate atmospheric mixing ratios of these species (additionally, we calculate mixing ratios based on Xe, see Sect. 4.3). The amount of air trapped within the ice sample is also used to calculate the total air content of the ice (Raynaud and Lebel, 1979). To this end, the bulk air leaving the *AirTrap* at −78 °C is re-collected on the *air volume trap* at −196 °C (SST tubing, 8 cm, o.d. 1/4″, i.d. 0.209″, filled with activated carbon; Fig. 1). Afterwards, the trap is isolated (VL1 and VL3 closed), heated to +80 °C, and the released gas is expanded into a thermally insulated 2-L volume by opening VL2. When the pressure reading is stable, pressure and temperature are read out, and mixing ratios of measured gas species are calculated vs. Σ_{air}, the sum of the bulk air components N_2, O_2, and Ar (see Sect. 4.4).

2.2 GC separation line

The GC line constitutes the continuous-flow part of our set-up (Fig. 1). Helium with 99.9990 % purity (Alphagaz I He; Carbagas, Gümligen, Switzerland) is used as carrier gas, and we further purify it using a high-capacity gas purifier, an inline gas purifier (both Supelco, Bellefonte, USA), and a custom made *purifier trap* held at −196 °C (SST, 30 cm, o.d. 1/4″, i.d. 0.209″, filled with activated carbon). The *purifier trap* is held at −196 °C during the week and warmed over the weekend for cleaning. The flow of the GC line is set to 1.0 mL min^{-1}.

AMTD
7, 2017–2069, 2014

When most of the bulk air components have been flushed from the *AirTrap*, valve 1 is switched from the vacuum line to the GC line, and the *AirTrap* is heated to 100 °C. The released gases are focussed for 22 min on the *cryofocus trap* (l = 90 cm, i.d. 0.32 mm GC-CarbonPlot, Agilent Technologies, USA) held at −115 °C. At this temperature the gases of interest are trapped while residual N_2, O_2, and CO are flushed into the GC.

Upon lifting the *cryofocus trap*, the gases of interest are released at ∼ 80 °C and transferred to the GC column (30 m GC-CarbonPlot). Compounds with a high affinity to the CarbonPlot column at 80 °C, like drill fluid, stay on the *cryofocus trap* (see Sect. 2.2.1). The GC temperature is held at 30 °C throughout the detection of CH_4, N_2O, and Xe. For the organic ppt-level species, temperature is increased at a rate of ca. 11 °C min^{-1}. The separated species leave the GC column at increasing retention time summarised in Table 1.

By switching valve 6 during the GC run, only CH_4 and Kr enter the loop containing the *combustion furnace,* as only CH_4 has to be oxidised to CO_2 prior to detection (Fig. 1). The construction of the *combustion furnace* is based on Bock et al. (2010a) with a ceramic tube filled with one wire each of Cu, Ni, and Pt (all wires are 0.1 mm o.d., Alfa Aesar, UK) and operated at 940 °C. We re-oxidise the *combustion furnace* every morning using the oxygen of the reference gas (Boulder). Since Kr has almost the same retention time in our system as methane, and doubly charged krypton ($^{86}Kr^{2+}$ = m/z 43) interferes with the CO_2 measurement producing erroneous results, these gases have to be separated (Schmitt et al., 2013). To provide sufficient separation between CH_4-derived CO_2 and Kr, a LN_2-trap ("S2", untreated fused silica capillary) is installed behind the outlet of the *combustion furnace* (Fig. 1). Here, the CH_4-derived CO_2 is trapped at −196 °C while Kr passes and enters the ion source well before the CH_4-derived CO_2 (Schmitt et al., 2013). A second LN_2-trap ("S1", untreated fused silica capillary) was installed before the *combustion furnace* to remove background CO_2 while CH_4 passes the trap. All other gases bypass the *combustion furnace* via valve 6 (Fig. 1).

AMTD
7, 2017–2069, 2014

To remove water vapour prior to the mass spectrometric detection, e.g. water formed from the combustion of methane, the He flow passes a *cold trap* (30 cm fused silica capillary, i.d. 0.32 mm, −70 °C).

2.2.1 Dealing with drill fluid residues

Deep ice cores are drilled with the help of so-called drill fluids, which are usually a mixture of hydrocarbons, e.g. kerosene and a densifier. The widely used densifier in the EPICA projects, at NGRIP and Talos Dome is HCFC-141b or $C_2H_3Cl_2F$ (Augustin et al., 2007). Problems during the analysis of ice cores caused by traces of drill fluid, which are enclosed in the ice during the drilling process are widespread and compromise the results of isotopic and trace gas measurements (Aydin et al., 2007; Schmitt et al., 2011; Rubino et al., 2013). During our first ice core measurements we encountered several instances of drill fluid contaminated samples, which led to baseline distortions and changes in the retention time of the species. Once in the GC, removing them is a tedious task. Therefore, a 6-port valve was installed, which prevents the drill fluid from entering the GC column in the first place (Fig. 1, valve 5). Valve 5 serves as a bypass for the GC flow. Once the gases of interest have been transferred from the heated *cryofocus trap*, valve 5 is switched to backflush the trap and to send the drill fluid to the vent. To achieve this, the *cryofocus trap* is heated to 160 °C using an infrared lamp (OSRAM, Augsburg, Germany). While this procedure removes the largest fraction of drill fluid components, a harmless, small part may still make its way into the GC and is monitored using its m/z 45 fragment $C_2H_2F^+$ in the run No. 7 (Table 1).

2.3 Inlet system and mass spectrometer

2.3.1 Inlet system

The GC system is connected to the mass spectrometer via an open split to introduce a constant fraction of sample. The inner diameter and length of the inlet capillary

AMTD
7, 2017–2069, 2014

(fused silica, i.d. 100 µm, length 150 cm) controls the flow rate to the ion source (ca. 0.3 mL min^{-1}). In routine operation the vacuum in the source chamber of the mass spectrometer is 2.6×10^{-6} mbar. A reference inlet system controls the injection of pure CO_2 and N_2O gas pulses into the mass spectrometer via SGE valves and a second inlet capillary (reference gas box, Elementar, Hanau, Germany), and a fraction is sucked into the ion source. The pure CO_2 ("Quellkohlensäure", Messer AG, Switzerland) has $\delta^{13}C$ and $\delta^{18}O$ values of -44.300 ± 0.005 ‰ vs. VPDB and 30.807 ± 0.067 ‰ vs. VSMOW, respectively (dual inlet measurements performed by P. Nyfeler). For the N_2O gas ("N_2O for medical use", Carbagas, Switzerland) the isotopic composition is unknown and both δ-values are set to 0.00 ± 0.00 ‰. In addition to serving as preliminary reference for the sample peaks, the on/off peaks admitted through this reference gas box are used to monitor the performance of the mass spectrometer and to correct for temporal drifts, where appropriate. Besides CO_2 and N_2O, rectangular Xe pulses (1.00 % Xe in He) are injected with our modified reference gas box to provide a reference for the Xe sample peak.

2.3.2 Continuous-flow IRMS

For the continuous-flow analyses we use an Isoprime IRMS (Elementar, Hanau, Germany). Our Isoprime is equipped with a universal triple collector plus two additional cups to monitor m/z 28 and 32, the N_2-cup and O_2-cup, respectively; details are described in Schmitt et al. (2013). This cup configuration allows for various source settings to analyse gas species of up to m/z 85 and, by chance, isotope analysis of doubly charged Xe isotopes.

The measurement of several gas species on a single sample requires that the IRMS is operated with different source tuning parameters and magnet current settings to accommodate the different m/z requirements. For each species or group of species a dedicated set of IRMS parameters and IonVantage scripts is selected, subsequently referred to as a run. To measure all species of a sample, we consecutively start individual runs, each run framing the peaks of the respective gas species (see Fig. 3).

AMTD
7, 2017–2069, 2014

Between the individual runs the IRMS source parameters are adjusted, requiring about 30 s to jump from one source setting to the next. Depending on the application, a sample measurement comprises a sequence of up to 7 runs (Table 1). The detection of Xe and CCl_2F_2 (run 2 and 6) requires that the magnet current is increased from its default value, 4000 nA, used for the CO_2-N_2O run, to 4800 nA leading to a transient warming of the magnet. To achieve stable peak centre conditions for the CO_2-N_2O run, the lengths of runs with deviating magnet currents are minimised, and the final run 7 (drill fluid components) again uses the CO_2-N_2O source setting. By the start of the next sample measurement, the magnet temperature has reached equilibrium and the IRMS is stable. The order of identified species passing our GC column is as follows: CH_4, Kr, CF_4, CO_2, N_2O, pentafluoroethane, ethyne, Xe, ethene, ethane, methyl chloride, propene, propane, and dichloro-difluoromethane (CCl_2F_2). We usually measure a sequence of runs with a selected number of target species as indicated in Table 1. From each run we obtain individual, mass-specific raw data files, which are processed individually.

For the CH_4-N_2O run the CO_2 cup configuration is used, collecting the major isotopologues of CO_2 and N_2O. Molecular nitrogen and oxygen are monitored using the N_2- and O_2-cups. All other species are measured at appropriate ions according to their mass spectra (National Institute of Standards, US: http://webbook.nist.gov/chemistry). For example, for both ethene and ethane, m/z 28 is the dominant ion in the mass spectra, but traces of background N_2 interferes at this m/z. Therefore, the less abundant m/z 27 ion is chosen, which allows the measurement of both gases in the same run. Besides these organic trace gas species, we measure the intensities of two Xe isotopes at m/z 66 and 68 reflecting the doubly charged ions $^{132}Xe^{2+}$ and $^{136}Xe^{2+}$, respectively, which is a novel application for CF-IRMS (see Fig. 4 and Sect. 4.2). To our knowledge this is the first time doubly charged Xe ions have been used for stable isotope analysis.

AMTD
7, 2017–2069, 2014

3 Analytical procedure

3.1 Sample material and preparation

Our experimental set-up is designed for analysing gas species from air extracted from ice core samples, bottled air samples, and working standard gases.

3.1.1 Ice preparation

The size of the measured ice core sample is ~ 160 g after about 40 g of ice from the surface is carefully removed in a first decontamination step. Possible lab air contamination at or close to the ice surface is removed by sublimation. This second decontamination step is achieved in the sample vessel at vacuum conditions by irradiating the ice sample several times for a few seconds using the heating bulbs. Using the LN_2 pumping system the sample vessel is kept cold at −5 °C throughout the time interval before the ice is melted and is stabilised at +3 °C after all ice is melted to keep pH_2O at ca. 7 mbar.

3.1.2 Air injection

Air samples are run via the bypass (see Sect. 2.1.1). Air cylinders need to be slightly overpressure to achieve a flow through the SGE valve of ca. 2 mL STP min^{-1}. The amount of gas injected into the vacuum system and trapped on the *AirTrap* is controlled by timing the opening of the SGE valve. An injection time of 24 min at a constant flow rate of 2 mL min^{-1} is equivalent to ca. 15–17 mL STP or ~ 160 g ice sample with entrapped air bubbles. Whole air working standards (externally or in-house calibrated gases) are also run using the bypass. We use three pressurised air cylinders to reference or check the performance of our measurements. The first cylinder CA08289 ("Boulder") contains present-day air with reduced CH_4 and N_2O mixing ratios of 1508.18 ± 0.17 ppb and 296 ± 11 ppb, respectively. The assigned δ^{13}C-CH_4 value for Boulder is −47.34 ± 0.02 ‰ and for δ^{15}N-N_2O and δ^{18}O-N_2O 7.55 ± 0.20 ‰

AMTD
7, 2017–2069, 2014

and 45.19 ± 0.28 ‰, respectively. The [CH_4] and δ^{13}C-CH_4 calibration was carried out by NOAA, Boulder, USA (n = 18) using CA03901 (1796.2 ± 0.7 ppb CH_4). The [N_2O] calibration was carried out by M. Baumgartner (n = 5) using NOAA reference gases (CA03901 315.1 ± 3.2 ppb N_2O). Cross-calibration for δ^{15}N-N_2O and δ^{18}O-N_2O via Air Controlé (see below) is linked to an atmospheric air cylinder from Groningen (NAT332, Sapart et al., 2011). Additionally, with respect to ethane, propane, and methyl chloride, our Boulder air standard is calibrated on the SIO-05 scale via J-155 by the Swiss Federal Laboratories for Materials Science and Technology (EMPA). The mixing ratios of ethane, propane, and methyl chloride in Boulder are 2916 ± 16 ppt, 1689 ± 9 ppt, and 418 ± 8 ppt, respectively. Boulder air is measured on a day-to-day basis together with samples and is used to calibrate samples to the international scales.

The second gas cylinder, CB541659 called "Air Controlé", also represents present day air and was filled by CarbaGas, Gümligen, Switzerland. The CH_4 and N_2O mixing ratios of 1971 ± 7 ppb and 327 ± 5 ppb, respectively, were determined using conventional gas chromatography (Flückiger et al., 2004). We measure Air Controlé only periodically to check long-term consistency of the other cylinders.

Our third gas cylinder is a synthetic gas mixture ("Saphir", No. 4405, CarbaGas, Switzerland) with a [CH_4] of 761 ppb, [N_2O] 315 ppb, [CO_2] 280 ppb, and [Xe] 90 ppb. It is measured on a daily basis.

3.2 Measurement scheme

The duration of a measurement varies with the numbers of species measured. The CH_4-N_2O-run (measuring m/z 44, 45, 46 for CH_4 and N_2O) takes ca. 80 min. A sequence with all runs (Table 1) takes 140 min. The routine protocol involving an ice sample is as follows: (1) working standard Boulder through the bypass, (2) working standard Saphir over ice, (3) blank over ice, (4) ice sample, treating all measurements almost identically (Werner and Brand, 2001). Measuring "over ice" means that Saphir is injected via the SGE valve into the vessel and pumped towards the *AirTrap*, while the

AMTD
7, 2017–2069, 2014

ice sample sits in the cold vessel at −5 °C throughout the procedure. The injection takes 24 min, i.e. the same duration as the injection of Boulder in the previous bypass measurement or the melting process of the ice in the subsequent measurement. Before the ice sample is melted and measured, we perform a whole-procedure blank run over ice (Sect. 3.2.1); this is an additional check whether the vessel is leak tight and provides an estimate for the blank correction. Finally, the ice sample is melted (Sect. 2.1.2) and measured.

3.2.1 Blank procedure and extraction efficiency

Treating a blank measurement identically to an ice sample measurement is the general idea of a whole-procedure blank. However, completely gas free "blank ice" is not available for our purposes, as it contains traces of the gas species we measure. Therefore, the best approximation of a whole-procedure blank is by measuring a blank over ice, called He blank. The temperature of the vessel stays at −5 °C throughout the He blank. We always process the same amount of He during a blank measurement and an ice sample measurement and use the same trapping time. All subsequent steps are identical for He blanks and ice sample measurements. The results of this blank measurement provide information on the cumulative blank for the procedure – the vacuum and trapping line and the continuous-flow GC line. That means that this blank is the sum of both air leaks and desorption within the system or bleed from the combustion oven and air released from the ice sample at a temperature of −5 °C in the vacuum system (around 0.1 g during the procedure).

Blank measurements using the bypass are valuable for mimicking sample or reference measurements and allow us to determine the location of leaks and outgassing contributions, e.g. with and without the contribution of the sample vessel. The bypass blank follows the same procedure as for He blank over ice measurements – except for bypassing the vessel.

To estimate the extraction efficiency, we run complete procedure blank measurements through the meltwater just after ice sample measurements. Generally, our

AMTD
7, 2017–2069, 2014

vacuum extraction guarantees an extraction efficiency of > 99.9 %, e.g. 99.98 % for CH_4 and of 99.97 % for Xe.

3.2.2 Measurement scheme for CH_4 and N_2O

Previous methods determining both CH_4 and N_2O isotopes on a single ice core sample either used two separate mass spectrometers for CH_4 and N_2O (Sapart et al., 2011) or two individual acquisitions on a single mass spectrometer (Sperlich et al., 2013). To our knowledge we are the first to combine these two isobaric species (CH_4-derived CO_2 and N_2O) in a single acquisition run. The acquisition of the CH_4-N_2O-run takes 4930 s and starts with three sets of rectangular and Gaussian peak pairs (Fig. 3a). The rectangular on/off peaks comprise pure N_2O and pure CO_2 injected via the reference box (Sect. 2.3.1). While the CO_2 on/off peak is injected, the GC-line status is set to "flow through the oven", and for the N_2O on/off peak, the valve 6 (Fig. 1) is switched to "bypass the oven" in order to have the same baseline conditions for rectangular and Gaussian peaks. Each pair of on/off peaks is followed by a pair of Gaussian peaks. The first peak is CH_4 (500 ppm CH_4 in He) injected into the GC-line via a 15 µL 1/16″ SST loop using valve 3 (Fig. 1). The second is N_2O (250 ppm N_2O in He), injected via a 13 µL loop using valve 4 (Fig. 1). Both loop fillings are trapped together on the *cryofocus trap* and released and transferred to the GC column as described above (Sect. 2.2). The three pairs of rectangular and Gaussian peaks are distributed over two thirds of the chromatogram (Fig. 3a) and allow for drift correction during the acquisition. The vacuum extraction and trapping process occur in parallel to this step (Sect. 2.1). After the gas or ice sample is transferred from the vacuum to the GC line, residual sample N_2 is the first signal to pass the cold *cryofocus trap* (Sect. 2.3.2). At the end of the acquisition, after the *cryofocus trap* is heated, the following peaks are observed according to their respective retention times (see Table 1): the sample Kr peak, the sample CH_4-derived CO_2 peak, and the sample N_2O peak (Fig. 3a). The separation of Kr and CH_4 is described in detail in Schmitt et al. (2013).

AMTD
7, 2017–2069, 2014

4 Data processing and corrections

The data processing is based on the mass-specific raw data files resulting from the sequence of runs for each measurement (see Sect. 2.3.2). The raw data files produced by IonVantage are processed by our own Matlab (MathWorks) routine, which calculates peak areas and raw isotopic ratios of the species. Isotope ratio calculations are performed for CH_4, N_2O, and Xe using Gaussian sample peaks, which are referenced in a first step to the rectangular on/off peaks for CO_2, N_2O, and Xe, respectively (see Sect. 2.3.1). Especially for the determination of the isotope ratios of N_2O, a robust background correction is crucial for high-precision measurements. As can be seen in Fig. 5, the intensities before the N_2O peak drop due to residual CO_2, which stems from both the preceding CH_4-derived CO_2 peak and residual sample CO_2. A robust, exponential fit of this long-term decay of the major signal can be obtained from the background before the peak, as the signal-to-noise ratio of the major signal is still high < 0.1 mV (black dots in Fig. 5). In contrast, fitting a sloping background on the minor1 and minor2 signals (red and blue lines showing a running mean, Fig. 5) is delicate, and the fit becomes more robust with the help of a background interval after the peak. With regard to the integration boundaries, the Matlab script is able to use either start and end slope criteria, fixed time steps left and right from the peak maximum or a fixed percentage of the intensity at peak maximum. The latter approach has resulted in the most reproducible values for N_2O.

In a second step, the individual runs of a species are assembled and analysed to calculate long-term trends. Calculations are carried out e.g. for the blank contribution to the sample peak area, the ppt-level species, trends in the isotopic ratios through time, and mixing ratios of the species based on air and Xe.

4.1 Blank estimation and correction

To achieve high-precision mixing ratios and isotopic ratios of trace gases in ice cores, low and quantifiable blank contributions are key aspects of the analytical routine. Firstly,

AMTD
7, 2017–2069, 2014

modern mixing ratios and isotopic ratios of the target species can be very different to those found in old ice core air, thus, contamination of lab air has to be minimised. Secondly, outgassing from the valve material and the extraction line is of critical concern.

To address both issues we follow two procedures. First we use whole procedure blank measurements, "He over ice", before each ice core sample to estimate the blank contribution for the following ice core sample. To further constrain the blank contribution, "He bypass" measurements are used. Secondly, we measure a contamination indicator of modern air directly with each sample as introduced by Aydin et al. (2010). Dichloro-difluoromethane, CCl_2F_2, is attractive for this purpose, since it currently has the highest mixing ratio of any man-made halocarbon with, about 550 ppt, and was absent in preindustrial times (Kaspers et al., 2004). Our detection limit for CCl_2F_2 is 1–2 ppt, thus, we can identify modern air contamination to the ice sample to a level of $\sim 0.3\,\%$ (volume fraction of ambient air relative to the ice core air). An example of a chromatogram for an ice core sample is shown in Fig. 3f, illustrating a CCl_2F_2 signal close to blank level (the ambient air signal intensity would be around 600 fA). For a typical ice core measurement, the CCl_2F_2 mixing ratio is 3 ± 2 ppt. Taken at face-value and using the ~ 550 ppt CCl_2F_2 in ambient air, this value translates into a contribution of $0.5 \pm 0.3\,\%$ ambient air volume to the air volume of the ice sample. However, this estimate is an upper boundary and relies on the assumption that CCl_2F_2 is co-transported within ambient air in a macroscopic leak. Generally, the measured CCl_2F_2 and other gas species of modern ambient air can result from various contamination types. First, ambient air can leak or diffuse into the extraction vessel and tubing which are at vacuum conditions. Secondly, modern air can be entrapped in ice core samples from depth ranges shortly below the firn-ice transition, where a small fraction of open porosity is still available for gas exchange. Aydin et al. (2010) dubbed this phenomenon post-coring entrapment of modern air and observed CCl_2F_2 in ice samples that were assumed to be fully closed-off (up to 20 m below the estimated firn-ice transition). Correspondingly, measuring CCl_2F_2 allows us to identify ice samples contaminated with modern air.

AMTD
7, 2017–2069, 2014

Overall, He over ice measurements give low blank values for CH_4 and N_2O, typically of about 2 ppb for CH_4 and 0.8 ppb for N_2O, which translates to only 0.4 % and 0.3 % of the average sample value (Table 2). The mixing ratios of the blank air (typically only 0.023 mL or 0.15 % of the air volume of an ice sample) for these species is around 1580 ppb for CH_4 and 581 ppb for N_2O. These CH_4 values could be explained by a mixture of air released from the ice sample containing air with typically low CH_4 (between 360 and 700 ppb) and a fraction of ambient air. In the case of N_2O, leaked lab air is another viable explanation if our lab air is heavily enriched in N_2O; however, a second source – outgassing from and permeation through polymer material used in the Vici valves – is more likely to occur, as blank values are relatively stable with time. For the organic ppt-level species, however, much higher blank values are observed and cause a sizeable fraction of the measured signals in ice core samples. For ethane, methyl chloride, and propane the observed He over ice blank values cannot be explained by a leak contribution from ambient air. The typical mixing ratios of the blank air are 41 400 ppt for ethane, 22 200 ppt for methyl chloride and 37 200 ppt for propane, thus orders of magnitude higher than ambient mixing ratios. Further tests using the bypass (Table 2, He through bypass) instead of the sample vessel showed that the blanks for these species result from outgassing of the valves rather than from the vessel itself. The Vici valves in particular contribute to this outgassing blank although their purge housings are permanently connected to a vacuum pump, which reduces the blank considerably.

Although the blank of a typical Antarctic ice core sample is considerable for ethane with 15 % and 18 % for propane and moderate with 6 % for methyl chloride, its level is relatively stable over a longer time window. This is to be expected if outgassing is the dominant process. Accordingly, the mixing ratio of a given trace gas is corrected for this contribution using the daily He over ice measurements by applying a spline interpolation similar to previous studies (Behrens et al., 2008). The mixing ratios reported in Tables 3 and 4 are blank-corrected.

AMTD
7, 2017–2069, 2014

4.2 Air content

The air content in ice samples is calculated using the read-out at the pressure gauge P3 for the *air volume* (Fig. 1), the weight of the ice sample, m_{ice}, the internal volume of the *air volume*, V_{air}, and a calibration factor, $f_{calibration}$.

$$V = p_{t\_corr} \cdot V_{air} / m_{ice} \cdot f_{calibration}$$

To compensate for temperature changes of the expansion volume, the pressure is first corrected for temperature changes, yielding p_{t_corr}. As the ice sample slowly sublimates prior to the melting and trapping process, a small fraction of the enclosed air is lost. The total loss is estimated to be around 0.5 over ice processing typically 0.023 mL air is collected and the corresponding time interval is 30 Since the internal volume of the *air volume* and its connections (Fig. 1) is not precisely known (ca. 1900 mL), calibration is necessary to yield accurate values comparable with other group' results. To determine the calibration factor, $f_{calibration}$, we use our measurements from the Dome C ice core and the accurately calibrated data from the same core (Raynaud et al., 2007). Our data set consists of 59 measurements and the overlapping calibration data comprise 54 points (Fig. 6). The calibration factor, $f_{calibration}$, is found by multiplying our data with a varying factor (between 0.98 and 1.02) and selecting the value where the sum of the differences of the time series is at a minimum. We estimate the uncertainty of this calibration procedure, i.e. the accuracy, to be 0.5 mL kg^{-1} by choosing random subgroups of both time series as input for the calibration. Regarding the achieved precision, Table 4 summarises results from two Antarctic ice cores: (1) vertical pairs of neighbouring samples from the "TALos Dome Ice CorE" (TALDICE) and (2) horizontal pairs from the shallow B34 core 75°0.15′ S, 00°4.104′ E, 2892 m a.s.l., Dronning Maud Land, drilled in the framework of the European Project for Ice Coring in Antarctica (EPICA)). The typical difference for horizontal pairs (B34) is 0.3 mL kg^{-1} and 0.6 mL kg^{-1} for vertical pairs (TALDICE), which is comparable to previous studies (Lipenkov et al., 1995).

AMTD
7, 2017–2069, 2014

4.3 Xe-based mixing ratios

Atmospheric mixing ratios are usually calculated by referencing the amount (mol) of a species to the amount of total air. However, if an atmospheric gas species is sufficiently constant over the relevant time scale, mixing ratios can be referenced to that parameter as well. In this respect the noble gas Xe can be used, as its past variations on the time scales considered here are smaller than a few permil, which is lower than our measurement precision (Headly and Severinghaus, 2007). Using this approach for ice core samples, the gravitational fractionation in the firn column has to be corrected for. Typically, the air at the bottom of the firn column is enriched in the heavier gas species by about 0.2 to 0.5 ‰ per mass unit (Craig et al., 1988; Landais et al., 2006). As the mass difference between e.g. ^{136}Xe and CH_4 is 120 mass units, the gravitational fractionation results in ratios which are up to 6 % lower than in the atmosphere. To quantify this gravitational effect, we use the Xe isotope ratio (^{136}Xe/^{132}Xe) measured with a precision of 0.05 ‰ per mass unit. Hence, we can correct each individual ice sample for gravitational enrichment, which is especially advantageous for ice cores with no available gravitational enrichment data. Our precision for the gravitational correction of 0.05 ‰ per mass unit obtained from δ^{136}Xe is lower than the results from dedicated systems for δ^{15}N (Landais et al., 2006), yet sufficient for our purpose here. Note that using ^{136}Xe/^{132}Xe to correct for gravitational effects of any gas species in the firn column assumes that the gravitational enrichment of the gases in the firn column only depends on the absolute mass difference of two species. Only in the case of kinetic fractionation processes for sites with large convective zones does this approach produce small biases (Kawamura et al., 2013). In fact, for Greenland ice cores, δ^{136}Xe/^{132}Xe is a better parameter to correct for the gravitational effect than the widely used $\delta^{15}N_2$, since thermal diffusion effects due to temperature gradients in the firn affect $\delta^{15}N_2$ more than δ^{136}Xe/^{132}Xe (Severinghaus et al., 2001).

The Xe-based mixing ratio of a sample, hereafter referred to e.g. as $^{Xe}[CH_4]_{sa\,raw}$, is derived from the ratio of the sample's species' peak area, $A(\text{species})_{sa}$, and the area

AMTD
7, 2017–2069, 2014

$A(^{136}Xe)_{sa}$ times the respective ratio of the reference, $A(\text{species})_{ref}$, and $A(^{136}Xe)_{ref}$ times the defined mixing ratio of the species of the reference, $[\text{species}]_{ref}$, following Eq. (1):

$$^{Xe}[\text{species}]_{sa\,raw} = A(\text{species})_{sa}/A(^{136}Xe)_{sa} \cdot A(\text{species})_{ref}/A(^{136}Xe)_{ref} \cdot [\text{species}]_{ref} \quad (1)$$

For each sample measurement we have a reference air measurement from the same day that could be used for a point-wise calculation of the mixing ratio. However, the reproducibility of the ice core replicates is better if a moving average of $A(\text{species})_{ref}/A(^{136}Xe)_{ref}$ over several days is used instead, which eliminates the stochastic measurement uncertainty in the daily reference air measurement.

In the following step the gravitational effect is corrected using the measured $^{136}Xe/^{132}Xe$ ratio of the sample times the mass difference between ^{136}Xe and the respective species, Δm:

$$^{Xe}[\text{species}]_{sa} = (1 - 1/4 \cdot \delta(^{136}Xe/^{132}Xe)_{sa} \cdot \Delta m/1000) \cdot {}^{Xe}[\text{species}]_{sa\,raw} \quad (2)$$

For calculating these mixing ratios we use our calibrated Boulder cylinder as reference (see Sect. 3.1.3 and Table 3). The thus derived Xe-based mixing ratios compare well with the mixing ratios based on air, (see Sect. 4.4 for a comparison of both mixing ratios). Note that the Xe-based mixing ratios cannot be used if the sample contains melt layers, because Xe is more soluble than the main air components (see below).

4.4 Air-based mixing ratios

The calculation of the air-based mixing ratios for a given species is similar to the calculation of the Xe-based mixing ratios. Instead of using Xe, the amount of air, Σair, serves as denominator in the following way:

$$[\text{species}]_{sa\,raw} = A(\text{species})_{sa}/\Sigma\text{air}_{sa} \cdot A(\text{species})_{ref}/\Sigma\text{air}_{ref} \cdot [\text{species}]_{ref} \quad (3)$$

AMTD
7, 2017–2069, 2014

Analogous to the Xe-based version, gravitational fractionation affects the air-based values and is corrected for using Xe isotopes. Here, Δm is the mass difference between the species and the average mol mass of air (28.8 u):

$$[\text{species}]_{\text{sa}} = (1 - 1/4 \cdot \delta(^{136}\text{Xe}/^{132}\text{Xe})_{\text{sa}} \cdot \Delta m/1000) \cdot [\text{species}]_{\text{sa raw}} \quad (4)$$

Together with the Xe-based mixing ratios from Sect. 4.3, our method allows for the calculation of atmospheric mixing ratios based on two approaches. To keep the figures and tables showing mixing ratios concise, only the air-based results are shown. For the raw mixing ratios, i.e. not corrected for gravitational effects in the firn ($[\text{species}]_{\text{sa raw}}$), the precision of both types of mixing ratios are comparable and the differences are within their combined errors. In contrast, for the CH_4 mixing ratios corrected for gravitational effects, the air-based values are more precise. The typical reproducibility for TALDICE replicates is 5 ppb for the air-based and 7 ppb for the Xe-based value. This is due to the uncertainty of the δ^{136}Xe measurement and the large mass difference between CH_4 (16 u) and Xe (136 u), compared to only 16 u and 28.8 u in case of the air-based [CH_4]. The 0.04 ‰ uncertainty of the δ^{136}Xe measurement and the mass difference of 120 u already lead to an uncertainty of 5 ‰ in the mixing ratio, e.g. 2.5 ppb for a concentration of 500 ppb.

4.5 Xe air ratio as melt layer proxy

To identify melt layers in polar ice several approaches can be applied. First, melt layers within bubble ice can be identified by visually analysing line scan profiles of the ice core (Abram et al., 2013). This technique works in the bubble ice zone in the absence of clathrates and is very sensitive as mm-thick melt layers can be reliably identified. Secondly, total air content measurements provide a proxy for melt layers and can be used to identify melt layers in deep clathrated ice as well (NEEM community members, 2013). This sensitivity to melt layer detection depends both on the analytical precision and the small-scale variability (mostly annual layering) of the total air content due to

AMTD
7, 2017–2069, 2014

changes in the firnification (Hörhold et al., 2012). Typically, the combined uncertainty of air content measurements is 1 % (Raynaud and Lebel, 1979). To identify melt layers from a reduced air content caused by melting, the "background air content" of unaffected bubble ice has to be established, which is primarily a function of the altitude (Raynaud and Lebel, 1979). The third principle uses the fact that some gases are more water-soluble than other gases, producing characteristic deviations in the mixing ratios of otherwise temporally fairly constant atmospheric gas species. Examples are the noble gases Ar, Kr, and Xe (Headly, 2008; NEEM community members, 2013). For the Greenland Dye 3 ice core, Headly (2008) reports δXe/Ar ratios for samples with melt layer sections which deviate by 50–100 ‰ from surrounding bubbly ice sections. The air content of these samples is reported to be reduced by 20–50 % compared to bubble ice. Instead of using δKr/Ar and δXe/Ar ratios, we calculate the parameter δXe/air for the same purpose using the gravitationally corrected mixing ratio of ^{136}Xe in air for the sample, $[^{136}\mathrm{Xe}]_{\mathrm{sa}}$, and for the reference, $[^{136}\mathrm{Xe}]_{\mathrm{ref}}$, applying the δ-notation as follows:

$$\delta\mathrm{Xe/air} = ([^{136}\mathrm{Xe}]_{\mathrm{sa}}/([^{136}\mathrm{Xe}]_{\mathrm{ref}} - 1) \cdot 1000 \quad (5)$$

The mixing ratio $[^{136}\mathrm{Xe}]_{\mathrm{ref}}$ is the value for ambient atmospheric air derived from measurements of Air Controlé. Note that for this purpose the small changes in the Xe content of the atmosphere due to changes in the ocean temperature can be neglected, as our error of 11 ‰ exceeds the small changes from this process, which amount to only ca. 2 ‰ (Headly, 2008; Ritz et al., 2011).

N_2 and O_2 have lower water solubilities than Ar (Weiss, 1970); thus, the sensitivity of δXe/air is higher than δXe/Ar. The drawback of using air as the denominator of the ratio is that air is a mixture of N_2, O_2, and Ar, with different water solubilities, yet dominated by the 79 % share of N_2 with a solubility of less than half of that of Ar. Our reproducibility of δXe/air for air samples is 10 ‰, and for ice samples without melt layers, typical differences of replicates are 8 ‰ (Table 4). A first feasibility study using Dye-III-88 ice core samples with and without melt layers has shown that our

AMTD
7, 2017–2069, 2014

δXe/air measurement is sensitive enough to detect melt layers (Fig. 7). With increasing melt fraction (estimated from visual core inspection) and decreasing air content, our δXe/air ratio increases. Roughly a 10 ‰ increase in δXe/air translates into a decrease of 2.8 mL kg^{-1} in air content. In view of measurement precision only, the air content measurement with a precision of < 1 mL kg^{-1} is more sensitive to detect melt layers than δXe/air. Yet, detecting melt layers via reduced air content alone requires knowledge of the expected air content of pure bubble ice as the air content at a drill site depends on several parameters (altitude, temperature, impurity content etc.), which gradually change over time. In contrast, anomalies in noble gas content, e.g. δXe/air, can be used to detect melt layers without further assumptions.

Figure 7 shows that CH_4 and especially N_2O are elevated in the melt layers as well. As the solubility of N_2O in water is higher than that of O_2 and N_2, elevated N_2O values are expected considering solubility effects alone (green and black bars in Fig. 7 showing the expected [N_2O] and [CH_4] values). Surprisingly, both δ^{13}C-CH_4 and the N_2O isotopes of the melt layer samples are indistinguishable to the bubble ice neighbours (Fig. 7). CH_4 in melt layer sections is higher than expected from solubility effects alone (black bars, Fig. 7) which could point to some in situ production in these samples, yet to a much smaller degree as reported previously (NEEM community members, 2013). Since δ^{13}C-CH_4 values are unaffected, this points either to an in situ signature close the atmospheric value, or the fact that CH_4 behaves differently to Xe during melt layer formation. This complicated picture among the different gas species observed from this small feasibility study on melt layers demonstrates that judgments based on a single parameter may lead to biased conclusions. Clearly, a more detailed investigation is necessary to characterise solubility effects and in situ production of CH_4 and N_2O in melt layers.

AMTD
7, 2017–2069, 2014

4.6 Isotope ratios of CH_4 and N_2O

4.6.1 Long-term trends and referencing to international standards

In a first step we reference our isotopic ratios for CH_4 and N_2O on a preliminary scale, which is a pure CO_2 working gas in the case of δ^{13}C-CH_4 and pure N_2O for δ^{15}N-N_2O and δ^{18}O-N_2O, both introduced as rectangular on/off peaks. To report our values on an international scale against a reference processed following the identical treatment principle (Werner and Brand, 2001), we use our Boulder measurements, which are processed on a daily basis. Similar to the calculation of the mixing ratios, the long-term evolution of the δ^{13}C-CH_4, δ^{15}N-N_2O and δ^{18}O-N_2O of the Boulder measurements are used for the correction to eliminate the stochastic measurement uncertainty in the daily values (see Fig. 8a). For δ^{13}C-CH_4, the correction is stable over time and amounts to only 0.04 ‰. We thus conclude that the overall isotopic fractionation in our system is very small. For previous methods more significant drifts in the measured δ^{13}C-CH_4 values were observed, presumably caused by the combustion unit (e.g. Behrens et al., 2008). In our case a time dependent correction did not further improve precision. For δ^{15}N-N_2O and δ^{18}O-N_2O we also observe that the isotopic ratios preliminarily referenced to our pure N_2O working gas do not vary over time, pointing to stable conditions in the overall preconcentration and measurement system.

4.6.2 Assessing amount effects

Tests regarding a possible dependency of the measured isotope ratios (δ^{13}C-CH_4, δ^{15}N-N_2O, and δ^{18}O-N_2O) on peak size were carried out with two contrasting air mixtures, Boulder and Saphir (see Table 3 for the respective isotopic and mixing ratios). While the isotopic signatures of Boulder are close to the range found in ice samples, the artificial Saphir mixture has strongly deviating δ^{13}C-CH_4, δ^{15}N-N_2O, and δ^{18}O-N_2O, which is ideal to check the system performance at strongly deviating isotope ratios. As mentioned above (Sect. 2.1.1), we simulate different sample sizes by timing the

AMTD
7, 2017–2069, 2014

opening of the SGE valve while keeping the flow rate to the vessel constant. To cover the peak size range from ca. 360 ppb CH_4 to ca. 1500 ppb, injection time for Boulder varies between 335 s and 1435 s. Since the isotopic signatures are so different between Boulder and Saphir, anomalies are calculated to plot the results of both gases in one graph (Fig. 8b and c). In general, no signal dependency on the respective peak size is observed for δ^{13}C-CH_4 and δ^{18}O-N_2O. For δ^{15}N-N_2O there is a small deviation towards lighter values for smaller sample sizes. Figure 8 shows that for δ^{13}C, precision is almost independent of sample size, while for δ^{15}N-N_2O and δ^{18}O-N_2O, precision is lower for the smallest peak size, which is, however, far outside the sample range indicated by the arrows.

5 System performance and reproducibility

In the following chapter we will discuss the precision of the overall system. We will concentrate in this discussion on the isotopic ratios of CH_4 and N_2O. The precision of the ppt-level concentration measurements is listed in Table 4 but is not discussed in the following, partly for the sake of conciseness of this paper, but mainly as the results on these species in polar ice cores is not limited by the analytical precision but by in situ production in the ice.

5.1 Pure gases

In the following we discuss the measurement precision of the different components in a sequential way starting with the isotope ratio mass spectrometer, the continuous-flow GC part, and finally the performance of the whole procedure. We use pure gases (CO_2 and N_2O) admitted via the reference gas box, CH_4 and N_2O mixtures in He injected onto the cryofocus, and whole air and ice core samples, respectively. Regarding the IRMS part only, the precisions of the three CO_2 and N_2O on/off peaks injected in each run (1σ-standard deviation of the three values after correcting for temporal

AMTD
7, 2017–2069, 2014

drift using a linear fit) are 0.03‰, 0.05‰, and 0.09‰ for $\delta^{13}C$, $\delta^{15}N$, and $\delta^{18}O$ respectively (Table 3, pure gases). For the Gaussian CH_4 and N_2O peaks we achieve precisions of 0.13‰, 0.22‰, and 0.43‰ for $\delta^{13}C$, $\delta^{15}N$, and $\delta^{18}O$ respectively. If the Gaussian peaks are corrected for the observed linear trend of the on/off peaks, precision improves slightly (Table 3, $gauss_{raw}$ and $gauss_{corr}$). The good precisions of these Gaussian peaks shows that both CO_2 and N_2O peaks can be measured within a run (see Fig. 3 for the injection scheme) without producing significant memory effects. This allows for the measurement of isotopic ratios of different isobaric species within a run, while previous studies measuring CH_4 and N_2O on a single sample either reserved a specific IRMS for each species (Sapart et al., 2011) or held one species until the IRMS was preconditioned for the second species (Sperlich et al., 2013). Currently, the CH_4 and N_2O Gaussian peaks within each chromatogram serve only to monitor the system performance and for troubleshooting. The reference basis for the CH_4 and N_2O sample peaks are the CO_2 and N_2O on/off peaks. When we tested to use the Gaussian peaks to correct sample peaks for any variable fractionation process in the GC part or the combustion oven, reproducibility of samples did not improve.

5.2 Whole air

For estimating the overall precision of our system we calculate the 1σ-standard deviation of our daily Boulder and Saphir measurements. For Boulder, we obtain standard deviations of 0.08‰, 0.23‰, and 0.56‰ for $\delta^{13}C$-CH_4, $\delta^{15}N$-N_2O, and $\delta^{18}O$-N_2O, respectively (Table 3). A similar precision for these parameters is obtained for Saphir, which is injected into the cold sample vessel containing the ice sample. As shown for our He over ice measurements, a small fraction of the ice sample sublimates during the "over ice" procedure, thus, air is released from the ice sample and "contaminates" the Saphir sample. Based on our He over ice blanks, the released amount of ice core air is 0.023 mL. With a Saphir sample volume of 13 mL, this translates to a volumetric contribution of 0.18 %. While the CH_4 and N_2O mixing ratios of Saphir are close to the

AMTD
7, 2017–2069, 2014

range of ice core samples, the isotopic ratios deviate considerably (Table 3). Yet the small contribution of ice core air does not significantly affect the isotopic signatures of [CH_4] or [N_2O]. In addition, two natural whole-air samples have been measured to quantify the reproducibility: Air Controlé and firn air from NEEM (Table 3).

5.3 Ice core replicates

Performance values derived from working standards and air samples allow a first approximation of the system performance due to identical treatment, yet determining the reproducibility on real ice samples is nevertheless necessary. One reason is that ice core samples may contain interferences, e.g. traces of drill fluid, which can affect some parameters. Second, the mixing ratios for CH_4, ethane, and propane in Antarctic ice cores, especially from cold periods, are considerably lower than those in the working standards. Two different approaches were applied. (1) We measured horizontal ice core replicates, i.e. samples from exactly the same depth and therefore identical gas and impurity content. For this we used ice from the shallow core B34 with the samples derived from two vertically neighbouring depth intervals (179.12–179.24 m and 179.24–179.36 m) with each interval providing four horizontal replicates. While most parameters show no difference among the two sections, air content and methyl chloride show differences (Tables 3 and 4). It is also notable that the ppt-level gas species for B34 show a higher variability when compared with TALDICE results, pointing to complex in situ production of these species in B34. (2) We measured vertical replicates on the TALDICE core. In this case, samples are vertical neighbours, i.e. the enclosed air has a slightly different age. The age difference, Δa, of our neighbouring samples depends on the specific depth due to thinning of the ice in the ice sheet. For our neighbouring samples Δa is between 50 and 250 years. In view of the width of the age distribution of the enclosed air (about 40 and 70 years for Holocene and glacial conditions respectively, B. Bereiter, personal communication, 2013), these vertical replicates are rather independent atmospheric samples than identical replicates. Two different bin classes ($\Delta a < 80$ years and < 250 years) were selected to account for

AMTD
7, 2017–2069, 2014

the different temporal variability of the parameters. From previous studies it is known that CH_4, a species with short atmospheric life times, shows high temporal variability, while e.g., δ^{15}N-N_2O, varies more gradually allowing wider binning, thus more samples are regarded replicates in this case. As expected, the reproducibility of most parameters is better for $\Delta a < 80$ years (Tables 3 and 4). For δ^{13}C-CH_4, δ^{15}N-N_2O, and δ^{18}O-N_2O the achieved reproducibility is better than in previous studies and also a step forward in terms of sample amount. Especially in terms of N_2O isotope ratios previous studies used around twice or three times as much ice as used in our method. For the ppt-level gas methyl chloride, the reproducibility is comparable to previous studies (Williams et al., 2007). In the case of ethane and propane, results from other studies are only available for Greenland ice cores, with their much higher Northern Hemisphere background concentrations (Aydin et al., 2007). For our Antarctic samples, the reproducibility for ethane obtained on B34, WAIS, and TALDICE ranges between 20 ppt for WAIS and 150 ppt for B34, i.e. amounts to 6 % and 30 % of the total signal, respectively. Yet, more critical is rather that the reconstructed absolute mixing ratios exceed the modern values and those reconstructed from firn air samples (Aydin et al., 2011). In situ production or reactions during the melting process for ethane and propane are the most likely explanations for the high levels at B34, WAIS, and TALDICE. As a conclusion for these two species, the blank contribution is an issue for further analytical improvements; however, the non-atmospheric component generated by the ice itself is a more severe problem, limiting its usage in reliably reconstructing past mixing ratios.

5.4 Intercomparison

In the following we compare our results with measurements from other laboratories, as for most measured parameters there is not yet an official reference available. However, air and ice sample intercomparison round-robins are currently underway. Given the large suite of parameters, not all measured species can be treated with the same detail here.

AMTD
7, 2017–2069, 2014

We lay special stress on δ^{13}C-CH_4, since several intercomparison samples have been measured by other groups as well, and only recently was an interference with Kr affecting several δ^{13}C-CH_4 data sets identified (Schmitt et al., 2013). Ice samples from the Antarctic ice core B34 (our δ^{13}C-CH_4 value: -47.10 ± 0.05 ‰) have also been measured previously by our colleagues at the Institute for Marine and Atmospheric Research Utrecht (IMAU) and at the Alfred Wegener Institute, Helmholtz Centre for Polar and Marine Research (AWI); Sapart et al. (2011) report δ^{13}C-CH_4 values of -46.46 ± 0.21 ‰ for IMAU and -46.57 ± 0.13 ‰ for AWI. Both values were measured before the awareness of the Kr issue. According to Schmitt et al. (2013), the Kr-correction would translate the IMAU and AWI numbers into lighter values, hence, closer to our value. A second ice core material allowing comparison with other groups is from the WAIS divide drill site (our WDCO5A core piece: bag 182, depth 170.99 m, ca. 1550 AD) provided by Todd Sowers from Penn State University (PSU). The Kr-corrected δ^{13}C-CH_4 values from neighbouring core sections from AWI is -47.81 ‰ (depth 166.78 m) and -48.28 ‰ (depth 164.96 m) and -47.87 ‰ (depth 169.80 m) for two pieces measured at PSU (Möller et al., 2013), thus close to our value of -48.03 ‰ (Table 3). Further support for the correctness of the Kr-corrected data recently published by Möller et al. (2013) comes from a remeasured time interval with a pronounced shift of 4 ‰ in δ^{13}C-CH_4, thus ideal to capture the dynamic range of the methods as well (Fig. 9). The Kr-corrected results measured on EDML and Vostok (Möller et al., 2013) fit well with our new data set from the TALDICE core taking the uncertainty of the age scales into account. Additionally, Fig. 9 allows for the comparison of the CH_4 mixing ratios obtained with different methods, all measured on the TALDICE core. Here, our [CH_4] results agree well with those of Buiron et al. (2011) as well as with a high-resolution data set using the continuous-flow analysis system, with a precision of 15–20 ppb (Schüpbach et al., 2011). Finally, we compare results from a firn air sample (canister name "FA23", depth 76 m deep, termed "firn air NEEM" in Tables 3 and 4) from the NEEM 2008 EU hole that has also been investigated by IMAU and the Centre for Ice and Climate, Copenhagen (CIC) (see Sapart et al., 2013). Our δ^{13}C-CH_4 value of -49.49 ± 0.04 ‰

AMTD
7, 2017–2069, 2014

agrees well with data from IMAU (Kr-corrected value, -49.69 ± 0.03 ‰) and CIC (no Kr issue, -49.52 ± 0.13 ‰).

As no official reference gas exists for the stable isotope ratios of N_2O, we tie our δ^{15}N-N_2O and δ^{18}O-N_2O values to those used at IMAU via Groningen air, NAT332. To assess the robustness of this single tie point NAT332, we compare results from three air samples that were provided and measured by CIC (Sperlich et al., 2013) and exchanged with our lab. For δ^{15}N-N_2O, our values for all three cylinders are heavier than the CIC values while our δ^{18}O-N_2O values are all lighter than CIC (Table 5). A second N_2O intercomparison using the "firn air NEEM" canister was conducted in collaboration with the laboratory at Oregon State University (OSU, Adrian Schilt). They tied their working standards for the N_2O isotope measurement to match the extrapolated values of the Cape Grim reconstruction (Park et al., 2012). For δ^{15}N-N_2O our value is again heavier by 0.8 ‰ compared to the OSU value and our δ^{18}O-N_2O of is again slightly lighter than OSU (Table 5). Regarding the N_2O mixing ratios, the two methods agree well, with our value at 289 ± 4 ppb and 291.2 ± 1.1 ppb for OSU. In both intercomparison cases our δ^{15}N-N_2O values turned out to be heavier by 0.2 to 0.8 ‰, whereas our δ^{18}O-N_2O values are lighter by 0.3 to 0.9 ‰.

Similar to δ^{13}C-CH_4, our WAIS divide intercomparison ice allows comparing with other groups' results. Our methyl chloride value of 889 ± 20 ppt is in accordance with measurements at University of Irvine (M. Aydin, personal communication, 2013) from neighbouring sections. A comparison of our TALDICE data from the Holocene with a recently published data set spanning the same period but measured on Taylor Dome ice (Verhulst et al., 2013) is delicate, since the variable difference in the two records points rather to in situ production.

AMTD
7, 2017–2069, 2014

6 Conclusions

We described a multi-parameter device to measure a large suite of trace gas species and their isotopic compositions on a single ice core sample and demonstrated its performance. The new system is based on an automated infrared melting device operated under vacuum, which allows for rapid extraction of the ice core air once released during the melting process. This principle combines high extraction efficiency with low helium consumption compared to techniques using a helium-purge set-up. A novel feature of our new device is the separation of drill fluid residues using a dedicated valve and backflush system.

With the help of our software routine developed in-house, we are able to calculate δ^{13}C-CH_4, and δ^{15}N-N_2O, and δ^{18}O-N_2O values within a single acquisition run. To prevent interference with Kr during the δ^{13}C-CH_4 measurement, Kr and CH_4-derived CO_2 are separated. Improvement in precision was reached for δ^{15}N-N_2O and δ^{18}O-N_2O analyses, which now allows us to reconstruct the small variations hidden within measurement uncertainty in previous studies.

To detect the other trace gas species (Xe, ethane, propane, methyl chloride, CCl_2F_2), we perform several peak jumps. Focussing the ion source to the m/z range of doubly charged Xe isotopes, we are the first to measure the isotopic composition on Xe^{2+} ions using GC-IRMS. The attained precision of 0.04 ‰ per mass unit allows us to correct the species' concentrations and isotopic ratios for gravitational effects in the firn column.

Acknowledgements. This work is a contribution to the European Project for Ice Coring in Antarctica (EPICA), a joint European Science Foundation/European Commission scientific program, funded by the EU (EPICA-MIS) and by national contributions from Belgium, Denmark, France, Germany, Italy, the Netherlands, Norway, Sweden, Switzerland and the UK, as well as to the "TALos Dome Ice CorE" (TALDICE) project funded by Italy, France, Germany, Switzerland and UK. The main EPICA logistic support was provided by IPEV and PNRA (at Dome C) and AWI (at Dronning Maud Land). Financial support for this work has been provided in part by the European Research Council Advanced Grant MATRICs, and the Schweizerischer Nationalfonds (SNF project primeMETHANE). B34 ice core samples were provided by the Alfred

AMTD
7, 2017–2069, 2014

Wegener Institute, Helmholtz Centre for Polar and Marine Research. We thank Matthias Baumgartner for measuring replicate ice core samples from the TALDICE core. Martin Vollmer from the Swiss Federal Laboratories for Materials Testing and Research (EMPA) kindly calibrated our working standard for the ppt-level species.

References

Abram, N. J., Mulvaney, R., Wolff, E., Triest, J., Kipfstuhl, S., Trusel, L. D., Vimeux, F., Fleet, L., and Arrowsmith, C.: Acceleration of snow melt in an Antarctic Peninsula ice core during the twentieth century, Nat. Geosci., 6, 404–411, doi:10.1038/ngeo1787, 2013.

Augustin, L., Panichi, S., and Frascati, F.: EPICA Dome C 2 drilling operations: performances, difficulties, results, Ann. Glaciol., 47, 68–72, 2007.

Aydin, M., De Bruyn, W. J., and Saltzman, E. S.: Preindustrial atmospheric carbonyl sulfide (OCS) from an Antarctic ice core, Geophys. Res. Lett., 29, 1359, doi:10.1029/2002gl014796, 2002.

Aydin, M., Williams, M. B., and Saltzman, E. S.: Feasibility of reconstructing paleoatmospheric records of selected alkanes, methyl halides, and sulfur gases from Greenland ice cores, J. Geophys. Res.-Atmos., 112, D07312, doi:10.1029/2006jd008027, 2007.

Aydin, M., Montzka, S. A., Battle, M. O., Williams, M. B., De Bruyn, W. J., Butler, J. H., Verhulst, K. R., Tatum, C., Gun, B. K., Plotkin, D. A., Hall, B. D., and Saltzman, E. S.: Post-coring entrapment of modern air in some shallow ice cores collected near the firn-ice transition: evidence from CFC-12 measurements in Antarctic firn air and ice cores, Atmos. Chem. Phys., 10, 5135–5144, doi:10.5194/acp-10-5135-2010, 2010.

Aydin, M., Verhulst, K. R., Saltzman, E. S., Battle, M. O., Montzka, S. A., Blake, D. R., Tang, Q., and Prather, M. J.: Recent decreases in fossil-fuel emissions of ethane and methane derived from firn air, Nature, 476, 198–201, doi:10.1038/nature10352, 2011.

Bazin, L., Landais, A., Lemieux-Dudon, B., Toyé Mahamadou Kele, H., Veres, D., Parrenin, F., Martinerie, P., Ritz, C., Capron, E., Lipenkov, V., Loutre, M.-F., Raynaud, D., Vinther, B., Svensson, A., Rasmussen, S. O., Severi, M., Blunier, T., Leuenberger, M., Fischer, H., Masson-Delmotte, V., Chappellaz, J., and Wolff, E.: An optimized multi-proxy, multi-site Antarctic ice and gas orbital chronology (AICC2012): 120–800 ka, Clim. Past, 9, 1715–1731, doi:10.5194/cp-9-1715-2013, 2013.

AMTD
7, 2017–2069, 2014

Behrens, M., Schmitt, J., Richter, K.-U., Bock, M., Richter, U., Levin, I., and Fischer, H.: A gas chromatography/combustion/isotope ratio mass spectrometry system for high-precision $\delta^{13}C$ measurements of atmospheric methane extracted from ice core samples, Rapid. Commun. Mass Sp., 22, 3261–3269, doi:10.1002/rcm.3720, 2008.

Bock, M., Schmitt, J., Behrens, M., Möller, L., Schneider, R., Sapart, C., and Fischer, H.: A gas chromatography/pyrolysis/isotope ratio mass spectrometry system for high-precision δD measurements of atmospheric methane extracted from ice cores, Rapid. Commun. Mass Sp., 24, 621–633, doi:10.1002/rcm.4429, 2010a.

Bock, M., Schmitt, J., Möller, L., Spahni, R., Blunier, T., and Fischer, H.: Hydrogen isotopes preclude marine hydrate CH_4 emissions at the onset of Dansgaard–Oeschger events, Science, 328, 1686–1689, doi:10.1126/science.1187651, 2010b.

Buiron, D., Chappellaz, J., Stenni, B., Frezzotti, M., Baumgartner, M., Capron, E., Landais, A., Lemieux-Dudon, B., Masson-Delmotte, V., Montagnat, M., Parrenin, F., and Schilt, A.: TALDICE-1 age scale of the Talos Dome deep ice core, East Antarctica, Clim. Past, 7, 1–16, doi:10.5194/cp-7-1-2011, 2011.

Craig, H., Horibe, Y., and Sowers, T.: Gravitational separation of gases and isotopes in polar ice caps, Science, 242, 1675–1678, 1988.

Faïn, X., Chappellaz, J., Rhodes, R. H., Stowasser, C., Blunier, T., McConnell, J. R., Brook, E. J., Preunkert, S., Legrand, M., Desbois, T., and Romanini, D.: High resolution measurements of carbon monoxide along a late Holocene Greenland ice core: evidence for in-situ production, Clim. Past Discuss., 9, 2817–2857, doi:10.5194/cpd-9-2817-2013, 2013.

Ferretti, D. F., Miller, J. B., White, J. W. C., Etheridge, D. M., Lassey, K. R., Lowe, D. C., Meure, C. M. M., Dreier, M. F., Trudinger, C. M., van Ommen, T. D., and Langenfelds, R. L.: Unexpected changes to the global methane budget over the past 2000 years, Science, 309, 1714–1717, doi:10.1126/science.1115193, 2005.

Flückiger, J., Blunier, T., Stauffer, B., Chappellaz, J., Spahni, R., Kawamura, K., Schwander, J., Stocker, T. F., and DahlJensen, D.: N_2O and CH_4 variations during the last glacial epoch: insight into global processes, Global Biogeochem. Cy., 18, GB1020, doi:10.1029/2003gb002122, 2004.

Headly, M. A.: Krypton and Xenon in Air Trapped in Polar Ice Cores: paleo-atmospheric Measurements for Estimating Past Mean Ocean Temperature and Summer Snowmelt Frequency, Ph.D. thesis, University of California, San Diego, 229 pp., 2008.

AMTD
7, 2017–2069, 2014

Hörhold, M. W., Laepple, T., Freitag, J., Bigler, M., Fischer, H., and Kipfstuhl, S.: On the impact of impurities on the densification of polar firn, Earth Planet. Sc. Lett., 325, 93–99, doi:10.1016/j.epsl.2011.12.022, 2012.

Kaspers, K. A., van de Wal, R. S. W., de Gouw, J. A., Hofstede, C. M., van den Broeke, M. R., van der Veen, C., Neubert, R. E. M., Meijer, H. A. J., Brenninkmeijer, C. A. M., Karlof, L., and Winther, J. G.: Analyses of firn gas samples from Dronning Maud Land, Antarctica: study of nonmethane hydrocarbons and methyl chloride, J. Geophys. Res.-Atmos., 109, D02307, doi:10.1029/2003jd003950, 2004.

Kawamura, K., Nakazawa, T., Aoki, S., Sugawara, S., Fujii, Y., and Watanabe, O.: Atmospheric CO_2 variations over the last three glacial-interglacial climatic cycles deduced from the Dome Fuji deep ice core, Antarctica using a wet extraction technique, Tellus B, 55, 126–137, doi:10.1034/j.1600-0889.2003.00050.x, 2003.

Kawamura, K., Severinghaus, J. P., Albert, M. R., Courville, Z. R., Fahnestock, M. A., Scambos, T., Shields, E., and Shuman, C. A.: Kinetic fractionation of gases by deep air convection in polar firn, Atmos. Chem. Phys., 13, 11141–11155, doi:10.5194/acp-13-11141-2013, 2013.

Landais, A., Barnola, J. M., Kawamura, K., Caillon, N., Delmotte, M., Van Ommen, T., Dreyfus, G., Jouzel, J., Masson-Delmotte, V., and Minster, B.: Firn-air $\delta^{15}N$ in modern polar sites and glacial-interglacial ice: a model-data mismatch during glacial periods in Antarctica?, Quaternary Sci. Rev., 25, 49–62, doi:10.1016/j.quascirev.2005.06.007, 2006.

Lipenkov, V., Candaudap, F., Ravoire, J., Dulac, E., and Raynaud, D.: A new device for the measurement of air content in polar ice, J. Glaciol., 41, 423–429, 1995.

Loulergue, L., Schilt, A., Spahni, R., Masson-Delmotte, V., Blunier, T., Lemieux, B., Barnola, J.-M., Raynaud, D., Stocker, T. F., and Chappellaz, J.: Orbital and millennial-scale features of atmospheric CH_4 over the past 800,000 years, Nature, 453, 383–386, doi:10.1038/nature06950, 2008.

Lüthi, D., Le Floch, M., Bereiter, B., Blunier, T., Barnola, J. M., Siegenthaler, U., Raynaud, D., Jouzel, J., Fischer, H., Kawamura, K., and Stocker, T. F.: High-resolution carbon dioxide concentration record 650,000–800,000 years before present, Nature, 453, 379–382, doi:10.1038/nature06949, 2008.

Melton, J. R., Whiticar, M. J., and Eby, P.: Stable carbon isotope ratio analyses on trace methane from ice samples, Chem. Geol., 288, 88–96, doi:10.1016/j.chemgeo.2011.03.003, 2011.

AMTD
7, 2017–2069, 2014

Möller, L., Sowers, T., Bock, M., Spahni, R., Behrens, M., Schmitt, J., Miller, H., and Fischer, H.: Independent variations of CH_4 emissions and isotopic composition over the past 160,000 years, Nat. Geosci., 6, 885–890, doi:10.1038/ngeo1922, 2013.

NEEM community members: Eemian interglacial reconstructed from a Greenland folded ice core, Nature, 493, 489–494, doi:10.1038/nature11789, 2013.

Park, S., Croteau, P., Boering, K. A., Etheridge, D. M., Ferretti, D., Fraser, P. J., Kim, K. R., Krummel, P. B., Langenfelds, R. L., van Ommen, T. D., Steele, L. P., and Trudinger, C. M.: Trends and seasonal cycles in the isotopic composition of nitrous oxide since 1940, Nat. Geosci., 5, 261–265, doi:10.1038/ngeo1421, 2012.

Pozzer, A., Pollmann, J., Taraborrelli, D., Jöckel, P., Helmig, D., Tans, P., Hueber, J., and Lelieveld, J.: Observed and simulated global distribution and budget of atmospheric C_2–C_5 alkanes, Atmos. Chem. Phys., 10, 4403–4422, doi:10.5194/acp-10-4403-2010, 2010.

Rahn, T. and Wahlen, M.: A reassessment of the global isotopic budget of atmospheric nitrous oxide, Global Biogeochem. Cy., 14, 537–543, doi:10.1029/1999gb900070, 2000.

Raynaud, D. and Lebel, B.: Total gas content and surface elevation of polar ice sheets, Nature, 281, 289–291, doi:10.1038/281289a0, 1979.

Raynaud, D., Lipenkov, V., Lemieux-Dudon, B., Duval, P., Loutre, M.-F., and Lhomme, N.: The local insolation signature of air content in Antarctic ice. A new step toward an absolute dating of ice records, Earth Planet. Sc. Lett., 261, 337–349, doi:10.1016/j.epsl.2007.06.025, 2007.

Rhodes, R. H., Fain, X., Stowasser, C., Blunier, T., Chappellaz, J., McConnell, J. R., Romanini, D., Mitchell, L. E., and Brook, E. J.: Continuous methane measurements from a late Holocene Greenland ice core: atmospheric and in-situ signals, Earth Planet. Sc. Lett., 368, 9–19, doi:10.1016/j.epsl.2013.02.034, 2013.

Ritz, S. P., Stocker, T. F., and Severinghaus, J. P.: Noble gases as proxies of mean ocean temperature: sensitivity studies using a climate model of reduced complexity, Quaternary Sci. Rev., 30, 3728–3741, doi:10.1016/j.quascirev.2011.09.021, 2011.

Rubino, M., Etheridge, D. M., Trudinger, C. M., Allison, C. E., Battle, M. O., Langenfelds, R. L., Steele, L. P., Curran, M., Bender, M., White, J. W. C., Jenk, T. M., Blunier, T., and Francey, R. J.: A revised 1000-year atmospheric $\delta^{13}C$-CO_2 record from Law Dome and South Pole, Antarctica, J. Geophys. Res.-Atmos., 118, 8482–8499, doi:10.1002/jgrd.50668, 2013.

Saito, T., Yokouchi, Y., Aoki, S., Nakazawa, T., Fujii, Y., and Watanabe, O.: A method for determination of methyl chloride concentration in air trapped in ice cores, Chemosphere, 63, 1209–1213, doi:10.1016/j.chemosphere.2005.08.075, 2006.

AMTD
7, 2017–2069, 2014

Saltzman, E. S., Aydin, M., Williams, M. B., Verhulst, K. R., and Gun, B.: Methyl chloride in a deep ice core from Siple Dome, Antarctica, Geophys. Res. Lett., 36, L03822, doi:10.1029/2008gl036266, 2009.
Sapart, C. J., van der Veen, C., Vigano, I., Brass, M., van de Wal, R. S. W., Bock, M., Fischer, H., Sowers, T., Buizert, C., Sperlich, P., Blunier, T., Behrens, M., Schmitt, J., Seth, B., and Röckmann, T.: Simultaneous stable isotope analysis of methane and nitrous oxide on ice core samples, Atmos. Meas. Tech., 4, 2607–2618, doi:10.5194/amt-4-2607-2011, 2011.
Sapart, C. J., Martinerie, P., Witrant, E., Chappellaz, J., van de Wal, R. S. W., Sperlich, P., van der Veen, C., Bernard, S., Sturges, W. T., Blunier, T., Schwander, J., Etheridge, D., and Röckmann, T.: Can the carbon isotopic composition of methane be reconstructed from multi-site firn air measurements?, Atmos. Chem. Phys., 13, 6993–7005, doi:10.5194/acp-13-6993-2013, 2013.
Schaefer, H. and Whiticar, M. J.: Measurement of stable carbon isotope ratios of methane in ice samples, Org. Geochem., 38, 216–226, doi:10.1016/j.orggeochem.2006.10.006, 2007.
Schilt, A., Baumgartner, M., Schwander, J., Buiron, D., Capron, E., Chappellaz, J., Loulergue, L., Schüpbach, S., Spahni, R., Fischer, H., and Stocker, T. F.: Atmospheric nitrous oxide during the last 140,000 years, Earth Planet. Sc. Lett., 300, 33–43, doi:10.1016/j.epsl.2010.09.027, 2010.
Schmitt, J.: A sublimation technique for high-precision $\delta^{13}C$ on CO_2 and CO_2 mixing ratio from air trapped in deep ice cores, University of Bremen, 2006.
Schmitt, J., Schneider, R., and Fischer, H.: A sublimation technique for high-precision measurements of $\delta^{13}CO_2$ and mixing ratios of CO_2 and N_2O from air trapped in ice cores, Atmos. Meas. Tech., 4, 1445–1461, doi:10.5194/amt-4-1445-2011, 2011.
Schmitt, J., Schneider, R., Elsig, J., Leuenberger, D., Lourantou, A., Chappellaz, J., Köhler, P., Joos, F., Stocker, T. F., Leuenberger, M., and Fischer, H.: Carbon isotope constraints on the deglacial CO_2 rise from ice cores, Science, 336, 711–714, doi:10.1126/science.1217161, 2012.
Schmitt, J., Seth, B., Bock, M., van der Veen, C., Möller, L., Sapart, C. J., Prokopiou, M., Sowers, T., Röckmann, T., and Fischer, H.: On the interference of Kr during carbon isotope analysis of methane using continuous-flow combustion–isotope ratio mass spectrometry, Atmos. Meas. Tech., 6, 1425–1445, doi:10.5194/amt-6-1425-2013, 2013.
Schüpbach, S., Federer, U., Bigler, M., Fischer, H., and Stocker, T. F.: A refined TALDICE-1a age scale from 55 to 112 ka before present for the Talos Dome ice core based on high-

AMTD
7, 2017–2069, 2014

resolution methane measurements, Clim. Past, 7, 1001–1009, doi:10.5194/cp-7-1001-2011, 2011.
Severinghaus, J. P., Grachev, A., and Battle, M.: Thermal fractionation of air in polar firn by seasonal temperature gradients, G-Cubed, 2, 146, doi:10.1029/2000GC000146, 2001.
Sowers, T., Alley, R. B., and Jubenville, J.: Ice core records of atmospheric N_2O covering the last 106,000 years, Science, 301, 945–948, doi:10.1126/science.1085293, 2003.
Sowers, T., Bernard, S., Aballain, O., Chappellaz, J., Barnola, J. M., and Marik, T.: Records of the $\delta^{13}C$ of atmospheric CH_4 over the last 2 centuries as recorded in Antarctic snow and ice, Global Biogeochem. Cy., 19, GB2002, doi:10.1029/2004GB002408, 2005.
Sperlich, P., Buizert, C., Jenk, T. M., Sapart, C. J., Prokopiou, M., Röckmann, T., and Blunier, T.: An automated GC-C-GC-IRMS setup to measure palaeoatmospheric $\delta^{13}C$-CH_4, $\delta^{15}N$-N_2O and $\delta^{18}O$-N_2O in one ice core sample, Atmos. Meas. Tech., 6, 2027–2041, doi:10.5194/amt-6-2027-2013, 2013.
Tschumi, J. and Stauffer, B.: Reconstructing past atmospheric CO_2 concentration based on ice-core analyses: open questions due to in situ production of CO_2 in the ice, J. Glaciol., 46, 45–53, 2000.
Veres, D., Bazin, L., Landais, A., Toyé Mahamadou Kele, H., Lemieux-Dudon, B., Parrenin, F., Martinerie, P., Blayo, E., Blunier, T., Capron, E., Chappellaz, J., Rasmussen, S. O., Severi, M., Svensson, A., Vinther, B., and Wolff, E. W.: The Antarctic ice core chronology (AICC2012): an optimized multi-parameter and multi-site dating approach for the last 120 thousand years, Clim. Past, 9, 1733–1748, doi:10.5194/cp-9-1733-2013, 2013.
Verhulst, K. R., Aydin, M., and Saltzman, E. S.: Methyl chloride variability in the Taylor Dome ice core during the Holocene, J. Geophys. Res.-Atmos., 118, 1–11, doi:10.1002/2013JD020197, 2013.
Vigano, I., Röckmann, T., Holzinger, R., van Dijk, A., Keppler, F., Greule, M., Brand, W. A., Geilmann, H., and van Weelden, H.: The stable isotope signature of methane emitted from plant material under UV irradiation, Atmos. Environ., 43, 5637–5646, doi:10.1016/j.atmosenv.2009.07.046, 2009.
Wang, Z., Chappellaz, J., Park, K., and Mak, J. E.: Large variations in Southern Hemisphere biomass burning during the last 650 years, Science, 330, 1663–1666, doi:10.1126/science.1197257, 2010.
Weiss, R. F.: The solubility of nitrogen, oxygen and argon in water and seawater, Deep-Sea Res., 17, 721–735, doi:10.1016/0011-7471(70)90037-9, 1970.

AMTD
7, 2017–2069, 2014

Werner, R. A. and Brand, W. A.: Referencing strategies and techniques in stable isotope ratio analysis, Rapid. Commun. Mass Sp., 15, 501–519, doi:10.1002/rcm.258, 2001.

Whiticar, M. and Schaefer, H.: Constraining past global tropospheric methane budgets with carbon and hydrogen isotope ratios in ice, Philos. T. R. Soc. A, 365, 1793–1828, doi:10.1098/rsta.2007.2048, 2007.

Williams, M. B., Aydin, M., Tatum, C., and Saltzman, E. S.: A 2000 year atmospheric history of methyl chloride from a South Pole ice core: evidence for climate-controlled variability, Geophys. Res. Lett., 34, L07811, doi:10.1029/2006gl029142, 2007.

Worton, D. R., Sturges, W. T., Reeves, C. E., Newland, M. J., Penkett, S. A., Atlas, E., Stroud, V., Johnson, K., Schmidbauer, N., Solberg, S., Schwander, J., and Barnola, J.-M.: Evidence from firn air for recent decreases in non-methane hydrocarbons and a 20th century increase in nitrogen oxides in the Northern Hemisphere, Atmos. Environ., 54, 592–602, doi:10.1016/j.atmosenv.2012.02.084, 2012.

Xiao, X., Prinn, R. G., Fraser, P. J., Simmonds, P. G., Weiss, R. F., O'Doherty, S., Miller, B. R., Salameh, P. K., Harth, C. M., Krummel, P. B., Porter, L. W., Mühle, J., Greally, B. R., Cunnold, D., Wang, R., Montzka, S. A., Elkins, J. W., Dutton, G. S., Thompson, T. M., Butler, J. H., Hall, B. D., Reimann, S., Vollmer, M. K., Stordal, F., Lunder, C., Maione, M., Arduini, J., and Yokouchi, Y.: Optimal estimation of the surface fluxes of methyl chloride using a 3-D global chemical transport model, Atmos. Chem. Phys., 10, 5515–5533, doi:10.5194/acp-10-5515-2010, 2010.

AMTD
7, 2017–2069, 2014

Table 1. Overview of measured gas species with their corresponding cup configurations for the seven individual acquisition runs (No.). Time is the elapsed time after the *cryofocus trap* is lifted, i.e. sample injected onto the GC column. GC (°C) denotes the temperature in the GC when the respective peak is detected in the IRMS.

No.	species	time (s)	GC (°C)	m/z major	m/z minor1	m/z minor2	remarks
1	Kr	414	30	44	45	46	Kr^+ and Kr^{2+} interference
	CH_4	441	30	44	45	46	combusted to CO_2, delayed by S2
	CO_2	~ 540	30	44	45	46	removed by S1 trap
	N_2O	586	30	44	45	46	
2	Xe	916	30		66	68	$^{132}Xe^{2+}$ and $^{136}Xe^{2+}$
3	C_2H_4	1020	57	–	–	27	$C_2H_3^+$
	C_2H_6	1212	118			27	$C_2H_3^+$
4	CH_3Cl	1592	166	–	–	50	$CH_3^{35}Cl^+$
5	C_3H_8	1730	177	–	–	29	$C_2H_5^+$
6	CCl_2F_2	1817	185	–	85	87	$C^{35}ClF_2^+$ and $C^{37}ClF_2^+$
7	$C_2H_3Cl_2F$	> 1900	> 200	–	45	–	$C_2H_2F^+$

AMTD
7, 2017–2069, 2014

Table 2. Results from three procedures to estimate the blank for measured gas species. Blanks are reported in three different units serving different purposes.

	He over ice; $n = 156$			He through bypass; $n = 6$			He through meltwater; $n = 8$		
species	(ppb[1])	(ppb[2])	(%[3])	(ppb[1])	(ppb[2])	(%[3])	(ppb[1])	(ppb[2])	(%[3])
air	–	–	0.15	–	–	0.02	–	–	0.02
CH_4	1580	2	0.4	7900	0.8	0.2	4300	1	0.2
N_2O	581	0.8	0.3	2100	0.3	0.1	3800	0.9	0.4
^{136}Xe	6200	10	0.1	nd	nd	nd	15 000	14	0.2
C_2H_6	41 400	65	15	350 000	50	11	1.4×10^6	281	63
CH_3Cl	22 200	35	6	190 000	21	4	19 000	35	9
C_3H_8	37 200	57	18	290 000	49	16	0.9×10^6	202	65
CCl_2F_2	1839	3	–	6000	8	–	12 000	2	–

[1] is the mixing ratio of a species. Note that due to the small amount of air involved in these blank measurements, the error due to pressure read out is around 10 %, dominating the error of these values.
[2] would be the increase in the sample mixing ratio if the measured amount of species were added to a typical ice sample (median of TALDICE samples, see Tables 3 and 4).
[3] is the percentage of the blank relative to a typical ice sample.
nd = not detectable.

AMTD
7, 2017–2069, 2014

Table 3. Means and 1σ standard deviations of isotope and mixing ratios of CH_4 and N_2O on gases and air extracted from ice samples. *n* denotes the number of measurements; reference values are in bold. Note that the isotopic ratios and mixing ratios for CH_4 and N_2O are without gravitational correction, i.e. they represent the composition of the trapped firn air in the ice core.

gas measured	*n*	CO_2 and CH_4-derived CO_2		N_2O		
		$\delta^{13}C$ (‰)	(ppb)	$\delta^{15}N$ (‰)	$\delta^{18}O$ (‰)	(ppb)
pure gases and mixtures in He						
rect on/off CO_2, N_2O	623	−44.30 ± 0.03		0.72 ± 0.05	37.93 ± 0.09	
$gauss_{raw}$ CH_4, N_2O	623	−41.80 ± 0.13		1.48 ± 0.22	38.92 ± 0.43	
$gauss_{corr}$ CH_4, N_2O	623	−41.84 ± 0.08		1.40 ± 0.17	38.82 ± 0.35	
working standards and air samples						
Boulder	–	**−47.34 ± 0.08**	**1508.2**	**7.55 ± 0.23**	**45.19 ± 0.56**	**296**
Saphir	141	−38.10 ± 0.16	761 ± 10	1.16 ± 0.25	38.12 ± 0.56	316 ± 3
Air Controlé	7	−47.79 ± 0.14	1977 ± 19	6.79 ± 0.27	43.31 ± 0.57	323 ± 3
Firn air NEEM	7	−49.49 ± 0.04	1275 ± 21	9.16 ± 0.19	44.91 ± 0.45	289 ± 4
ice core samples						
B34 (179.12 m)	4	−47.12 ± 0.05	636 ± 9	10.75 ± 0.09	45.84 ± 0.80	261 ± 2
B34 (179.24 m)	4	−47.08 ± 0.05	648 ± 12	10.88 ± 0.24	45.32 ± 0.46	262 ± 4
TALDICE[1] (Δa < 80 a)	14	−48.56 ± 0.10	556 ± 5	10.88 ± 0.22	45.95 ± 0.28	259 ± 2
TALDICE[1] (Δa < 250 a)	21	−48.18 ± 0.17	535 ± 5	10.96 ± 0.21	45.92 ± 0.32	254 ± 3
WAIS (170.99 m)	4	−48.03 ± 0.08	710 ± 9	10.32 ± 0.14	45.92 ± 0.46	265 ± 2

[1] For TALDICE the replicate means are shown to put the measured reproducibility into perspective; the reported mean for each parameter is the average of all replicate pairs of the measured time interval (2 kyr to 100 kyr). Note, the reproducibility (± value) for TALDICE samples represent the average standard deviation of pairs of "vertical neighbouring replicates"; see Sect. 5.3 for details.

AMTD
7, 2017–2069, 2014

Table 4. Means and 1σ standard deviations of isotope and mixing ratios on trace gases and air extracted from ice samples. Reference values are in bold. δ^{136}Xe denotes the deviation of the $^{136}Xe/^{132}Xe$ ratio against the standard divided by 4 to express the δ per 1 mass difference. δXe/air is the anomaly of the atmospheric Xe mixing ratio with respect to the standard in ‰. Note that CCl_2F_2 is absent in the pre-industrial air, and the reported values for ice samples are contamination blank. See caption Table 3 for further information.

gas measured	*n*	δ^{136}Xe (‰)	δXe/air (‰)	C_2H_6 (ppt)	CH_3Cl (ppt)	C_3H_8 (ppt)	CCl_2F_2 (ppt)	air content (mL kg^{-1})
working standards and air samples								
Boulder	–	–	–	**2916 ± 16**	**418 ± 8**	**1689 ± 9**	**405 ± 10**	–
Saphir	141	0.03 ± 0.06	105 ± 10					–
Air Controlé	7	**0.02 ± 0.07**	**0 ± 10**	2558 ± 79	456 ± 17	1792 ± 68	513 ± 11	–
Firn air NEEM	7	0.24 ± 0.06	13 ± 6	2117 ± 25	499 ± 24	612 ± 30	32 ± 1	–
ice core samples								
B34 (179.12 m)	4	0.43 ± 0.04	12 ± 8	474 ± 151	503 ± 33	325 ± 115	3 ± 2	90.9 ± 0.3
B34 (179.24 m)	4	0.47 ± 0.07	9 ± 4	418 ± 120	561 ± 26	289 ± 93	3 ± 2	93.7 ± 0.4
TALDICE (Δa < 80 a)	14	0.34 ± 0.04	15 ± 7	351 ± 77	511 ± 19	209 ± 54	3 ± 2	100.9 ± 0.8
TALDICE (Δa < 250 a)	21	0.38 ± 0.05	13 ± 8	353 ± 63	530 ± 24	204 ± 78	3 ± 2	101.4 ± 0.7
WAIS (170.99 m)	4	0.30 ± 0.04	5 ± 14	345 ± 21	889 ± 20	297 ± 52	2 ± 1	111.5 ± 0.4

AMTD
7, 2017–2069, 2014

Table 5. Intercomparison of isotope measurements on N_2O of air cylinders between this study (Bern) and published data from CIC (Sperlich et al., 2013) and OSU (A. Schilt, personal communication, 2013). The differences (diff.) are calculated between Bern and the external results.

cylinder name	δ^{15}N-N_2O (‰)			δ^{18}O-N_2O (‰)		
	Bern	CIC	diff.	Bern	CIC	diff.
NEEM[1]	6.97 ± 0.08	6.49 ± 0.04	0.48	43.52 ± 0.39	44.58 ± 0.06	−1.06
AL[1]	1.57 ± 0.47	1.01 ± 0.15	0.56	38.15 ± 0.39	38.80 ± 0.40	−0.65
NOAA[1]	−0.28 ± 0.18	−0.46 ± 0.15	0.18	40.25 ± 0.53	41.06 ± 0.40	−0.81
Firn air NEEM FA32	9.16 ± 0.19	8.36 ± 0.12	0.80	44.91 ± 0.45	45.28 ± 0.29	−0.37

[1] Same names as used in Sperlich et al. (2013).

AMTD
7, 2017–2069, 2014

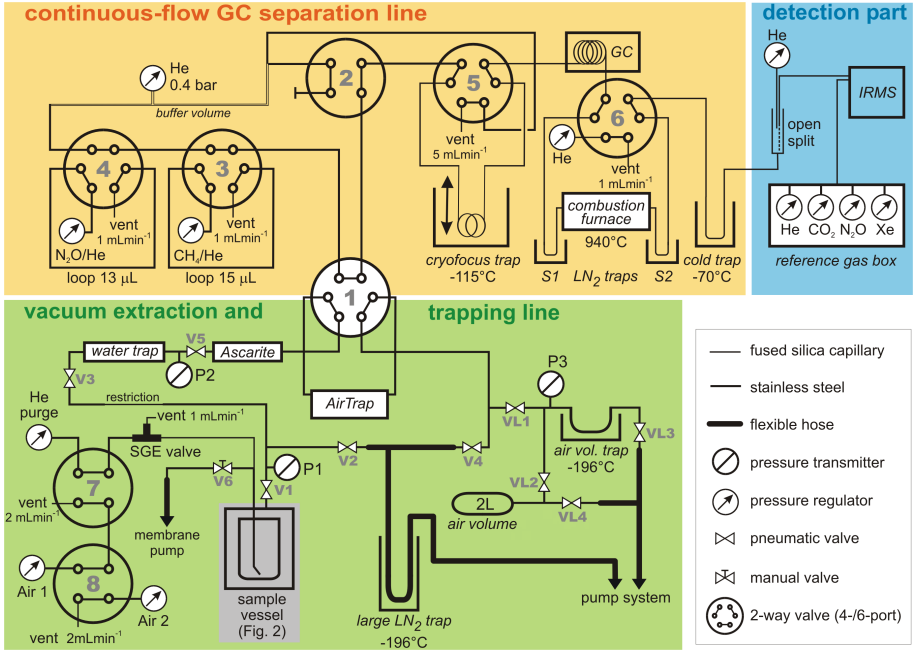

Fig. 1. Custom-built analytical set-up comprising the vacuum extraction and trapping line (green), the continuous-flow line with the gas chromatograph (GC) and the combustion furnace (orange), and the detection part (blue). The sample vessel (shaded grey) is sketched in detail in Fig. 2.

AMTD
7, 2017–2069, 2014

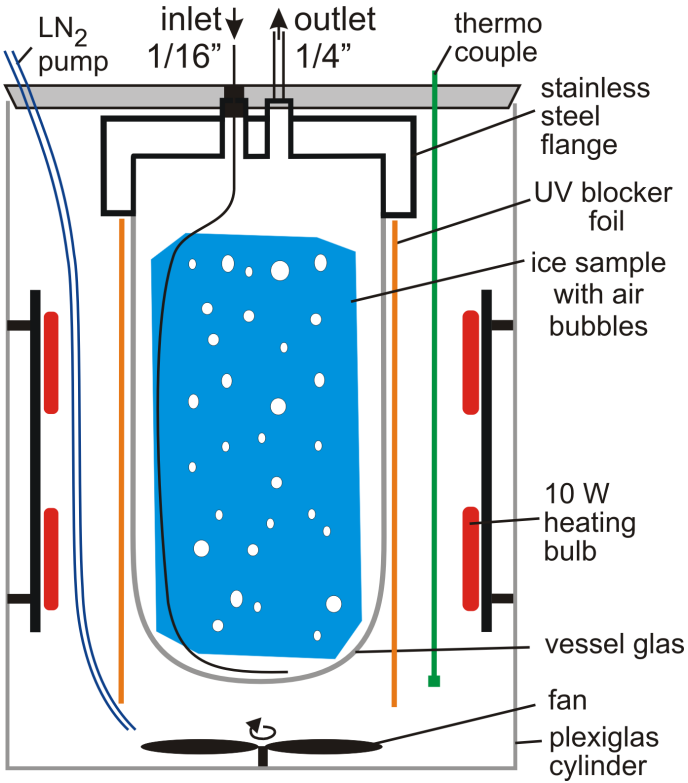

Fig. 2. Custom-built vessel holder with sample glass vessel to automatically melt ice samples using infrared light (heating bulbs + UV light blocker foil) or to keep the ice at around −5 °C using LN_2 during pumping and procedure blank processing.

AMTD
7, 2017–2069, 2014

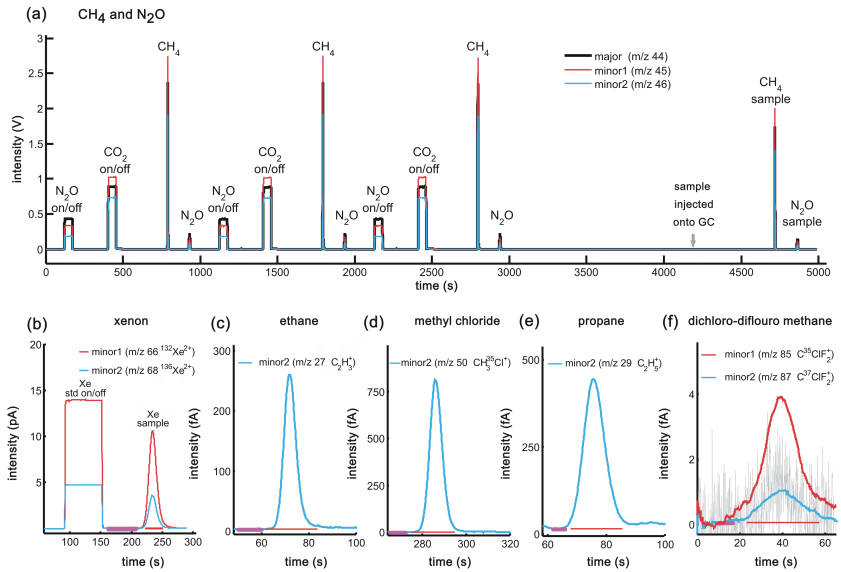

Fig. 3. Chromatograms illustrating the sequence of runs and detected gas species at the respective focus settings of the ion source for an Antarctic ice core sample. The order from **(a)** to **(f)** follows the increasing retention time starting with CH_4 and ending with CCl_2F_2. **(a)** CH_4-N_2O-run consisting of rectangular on/off peaks for N_2O and CO_2 admitted by the reference gas box, Gaussian peaks for CH_4 and N_2O injected via valves 3 and 4 (Fig. 1), and sample peaks for CH_4 and N_2O at the end of the run. **(b)** Xe run consisting of a rectangular on/off Xe peak as reference and the following Xe sample peak. **(c–f)** show the chromatograms for the organic trace gas species ethane, methyl chloride, propane, and dichloro-difluoro-methane (CCl_2F_2), respectively, eluting at higher GC temperatures. All chromatograms reflect species concentrations of the ice, besides CCl_2F_2, which serves as an indicator of contamination with modern ambient air. Note, to better visualise the small CCl_2F_2 intensities from the highly amplified minor1 and minor2 cups, the red and blue lines here represent a moving average of 1 s; the minor2 raw signal at 0.1 s resolution is shown as a grey line.

AMTD
7, 2017–2069, 2014

CH4, N2O and Xe isotopes and mixing ratios from a single ice sample

J. Schmitt et al.

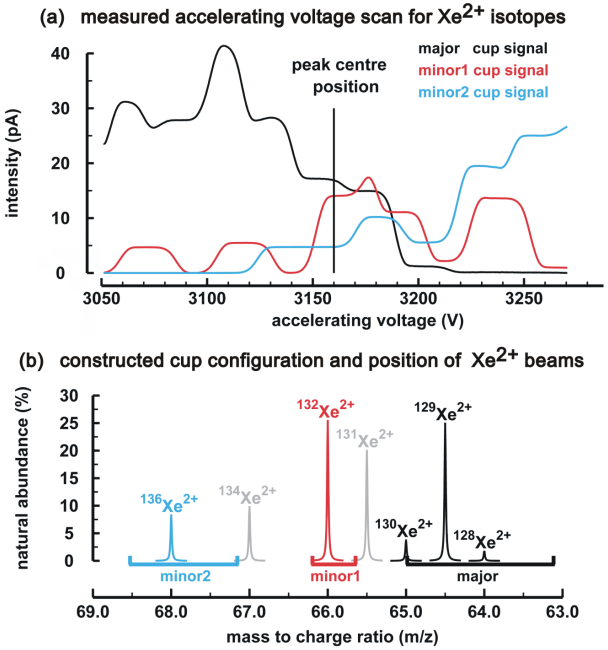

Fig. 4. Mass spectrometer focussing to allow for isotope analysis of doubly charged Xe ions. **(a)** Accelerating voltage scan (note the magnet current was switched from 4000 nA to 4800 nA to allow for the collection of higher m/z ions in the cups) over the region where Xe^{2+} ions hit the Faraday cups. At the selected peak centre position a shared plateau region and the subsequent stable measurement conditions allow for the simultaneous detection of $^{136}Xe^{2+}$ in minor2 and $^{132}Xe^{2+}$ in minor1 to calculate isotope ratios spanning 4 m/z units. **(b)** Constructed Faraday cup configuration at peak centre position illustrates that the centre position has to be selected carefully as many Xe^{2+} ions are close to cup edges. Note, the mass to charge ratio of **(b)** is plotted on an inverse scale to directly correspond to **(a)**.

AMTD
7, 2017–2069, 2014

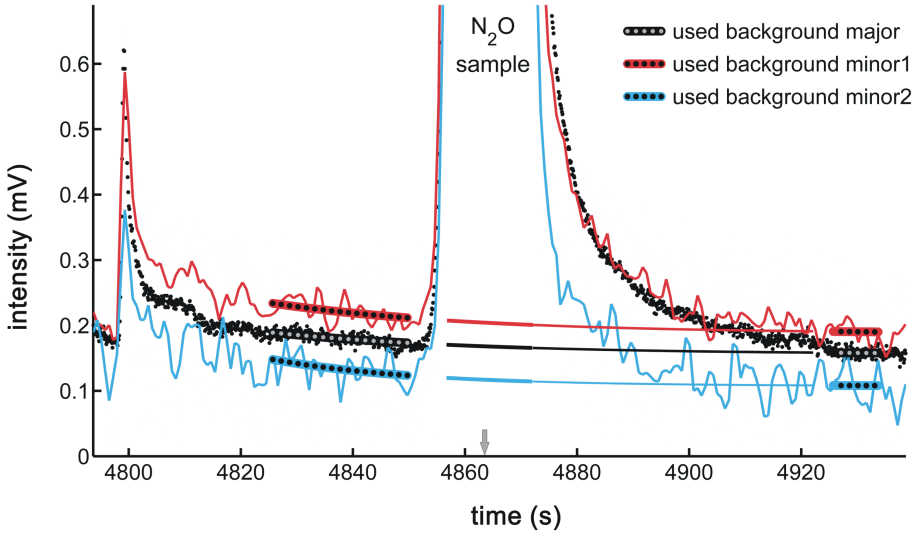

Fig. 5. Zoom into the background region of the N_2O sample peak (peak maximum indicated by the arrow). For clarity, the minor1 and minor2 signals are plotted as a 1.5 s moving average to allow for following the faint trends. For the background correction, an exponential fit is calculated using background data before and after the N_2O peak (dotted intervals). The thick solid lines below the N_2O peak indicate the subtracted background signals. Thin lines connect the background below the N_2O peak with the background region after the peak to visually examine the quality of the fitting step.

AMTD
7, 2017–2069, 2014

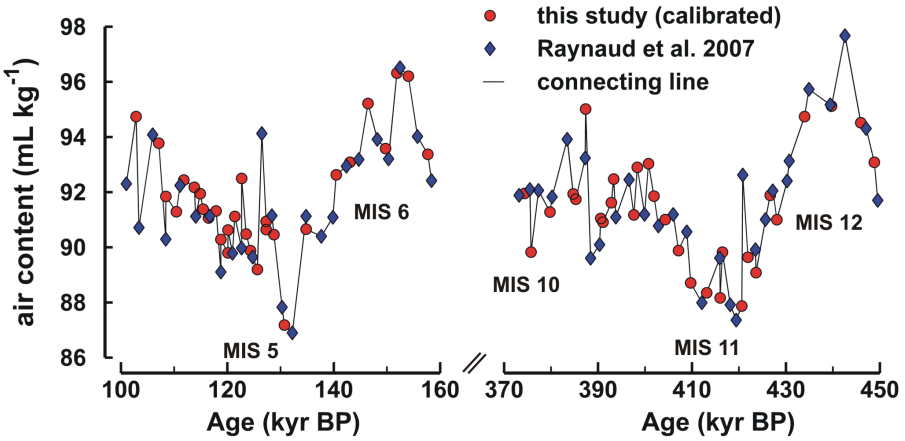

Fig. 6. Comparison of our calibrated air content measurements from the Dome C core with published results from the same ice core (Raynaud et al., 2007) plotted on the AICC2012 ice age scale (Bazin et al., 2013; Veres et al., 2013).

AMTD
7, 2017–2069, 2014

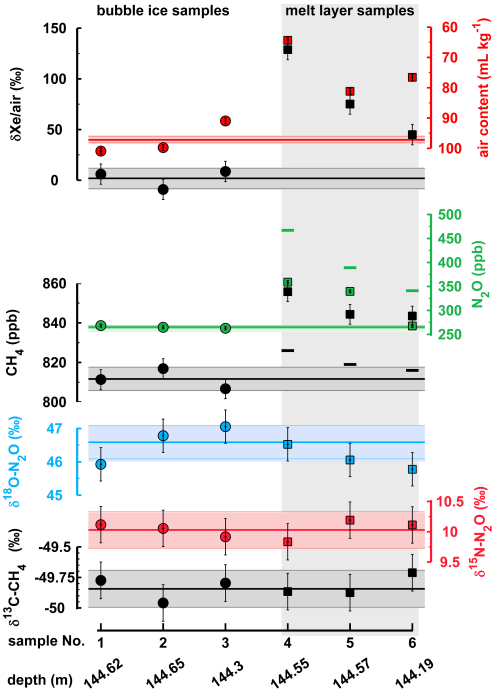

Fig. 7. Results of ice core measurements (Dye 3-88, bag 145, depth is given as top of sample) with sections of bubble ice and sections including melt layers. Samples consisting of bubble ice only (No. 1–3) are shown as circles and samples with melt layers (No. 4–6) are shown as squares within grey shading. Note that air content is plotted on an inverse axis. For CH_4 and N_2O, green and black bars, respectively, indicate calculated values in the melt layer samples assuming that both species are affected by equilibrium solubility effects as derived from the δXe/air anomaly. Error bars represent the average standard deviation derived from replicate samples (see Table 3). Horizontal shading and lines in the respective species' colour represent the mean of the bubble ice measurements and 1σ of the typical reproducibility (Tables 3 and 4).

AMTD
7, 2017–2069, 2014

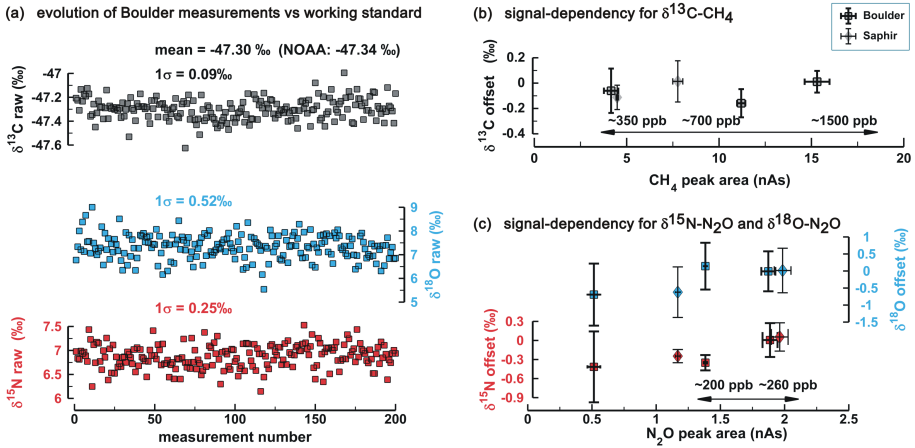

Fig. 8. System performance of reference air measurements. **(a)** Long-term evolution of the measured raw values for the isotopic signatures (δ^{13}C, δ^{15}N, δ^{18}O) of Boulder air referenced against pure CO_2 and N_2O on/off peaks spanning a period of 1 year. Effect of sample size and signal intensity on the measured isotope ratios **(b)** for δ^{13}C-CH_4 and **(c)** for δ^{18}O-N_2O and δ^{15}N-N_2O. Within the range covered by ice core and ambient air samples, all three isotope ratios are independent of the signal intensity.

AMTD
7, 2017–2069, 2014

CH4, N2O and Xe isotopes and mixing ratios from a single ice sample

J. Schmitt et al.

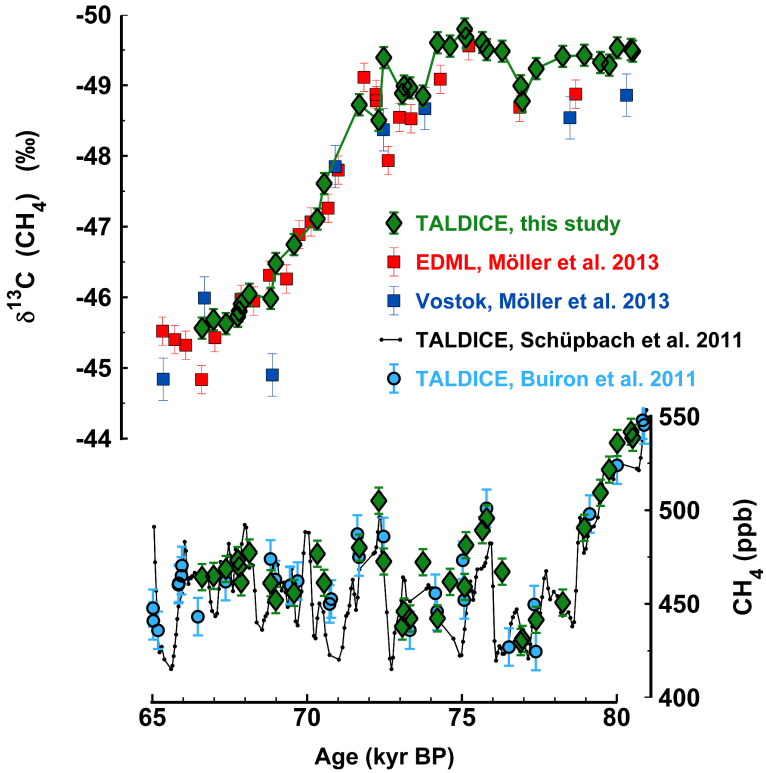

Fig. 9. Comparison of our δ^{13}C-CH_4 and [CH_4] measurements with published results for an interval showing strong variations in both parameters. All data are plotted on a common age scale (Veres et al., 2013).

AMTD
7, 2017–2069, 2014